

## Land Cover Control on the Drivers of Evaporation and Sensible Heat Fluxes An Observation-Based Synthesis for the Netherlands

Jansen, Femke A.; Jongen, Harro J.; Jacobs, Cor M.J.; Bosveld, Fred C.; Buzacott, Alexander J.V.; Heusinkveld, Bert G.; Kruijt, Bart; van der Molen, Michiel; Uijlenhoet, Remko; More Authors

**DOI**

[10.1029/2022WR034361](https://doi.org/10.1029/2022WR034361)

**Publication date**

2023

**Document Version**

Final published version

**Published in**

Water Resources Research

**Citation (APA)**

Jansen, F. A., Jongen, H. J., Jacobs, C. M. J., Bosveld, F. C., Buzacott, A. J. V., Heusinkveld, B. G., Kruijt, B., van der Molen, M., Uijlenhoet, R., & More Authors (2023). Land Cover Control on the Drivers of Evaporation and Sensible Heat Fluxes: An Observation-Based Synthesis for the Netherlands. *Water Resources Research*, 59(11), Article e2022WR034361. <https://doi.org/10.1029/2022WR034361>

**Important note**

To cite this publication, please use the final published version (if applicable).  
Please check the document version above.

**Copyright**

Other than for strictly personal use, it is not permitted to download, forward or distribute the text or part of it, without the consent of the author(s) and/or copyright holder(s), unless the work is under an open content license such as Creative Commons.

**Takedown policy**

Please contact us and provide details if you believe this document breaches copyrights.  
We will remove access to the work immediately and investigate your claim.

# Water Resources Research®



## RESEARCH ARTICLE

10.1029/2022WR034361

### Key Points:

- The drivers of latent and sensible heat fluxes in the Netherlands were studied over various land cover types based on regression analyses
- Drivers of evaporation associated with energy availability, water availability, exchange efficiency vary substantially per land cover type
- In natural landscape mosaics limitation of evaporation by water availability, energy availability and exchange efficiency coexist

### Correspondence to:

A. J. Teuling,  
[ryan.teuling@wur.nl](mailto:ryan.teuling@wur.nl)










### Citation:

Jansen, F. A., Jongen, H. J., Jacobs, C. M. J., Bosveld, F. C., Buzacott, A. J. V., Heusinkveld, B. G., et al. (2023). Land cover control on the drivers of evaporation and sensible heat fluxes: An observation-based synthesis for the Netherlands. *Water Resources Research*, 59, e2022WR034361. <https://doi.org/10.1029/2022WR034361>

Received 23 DEC 2022

Accepted 1 SEP 2023

## Land Cover Control on the Drivers of Evaporation and Sensible Heat Fluxes: An Observation-Based Synthesis for the Netherlands

Femke A. Jansen<sup>1</sup> , Harro J. Jongen<sup>1,2</sup> , Cor M. J. Jacobs<sup>3</sup> , Fred C. Bosveld<sup>4</sup> , Alexander J. V. Buzacott<sup>5</sup>, Bert G. Heusinkveld<sup>2</sup>, Bart Kruijt<sup>6</sup> , Michiel van der Molen<sup>2</sup>, Eddy Moors<sup>5,7</sup> , Gert-Jan Steeneveld<sup>2</sup> , Christiaan van der Tol<sup>8</sup> , Ype van der Velde<sup>5</sup>, Bernard Voortman<sup>9</sup>, Remko Uijlenhoet<sup>10</sup>, and Adriaan J. Teuling<sup>1</sup> 

<sup>1</sup>Hydrology and Quantitative Water Management Group, Wageningen University and Research, Wageningen, The Netherlands, <sup>2</sup>Meteorology and Air Quality Section, Wageningen University and Research, Wageningen, The Netherlands, <sup>3</sup>Wageningen Environmental Research, Wageningen University and Research, Wageningen, The Netherlands, <sup>4</sup>Royal Netherlands Meteorological Institute, De Bilt, The Netherlands, <sup>5</sup>Faculty of Science, Department of Earth Sciences, Vrije Universiteit Amsterdam, Amsterdam, The Netherlands, <sup>6</sup>Earth System Science Group, Wageningen University and Research, Wageningen, The Netherlands, <sup>7</sup>IHE Delft Institute for Water Education, Delft, The Netherlands, <sup>8</sup>Faculty of ITC, University of Twente, Enschede, The Netherlands, <sup>9</sup>Moisture Matters, Utrecht, The Netherlands, <sup>10</sup>Department of Water Management, Delft University of Technology, Delft, The Netherlands

**Abstract** Land cover controls the land-atmosphere exchange of water and energy through the partitioning of solar energy into latent and sensible heat. Observations over all land cover types at the regional scale are required to study these turbulent flux dynamics over a landscape. Here, we aim to study how the control of daily and midday latent and sensible heat fluxes over different land cover types is distributed along three axes: energy availability, water availability and exchange efficiency. To this end, observations from 19 eddy covariance flux tower sites in the Netherlands, covering six different land cover types located within the same climatic zone, were used in a regression analysis to explain the observed dynamics and find the principle drivers. The resulting relative position of these sites along the three axes suggests that land cover partly explains the variance of daily and midday turbulent fluxes. We found that evaporation dynamics from grassland, peatland swamp and cropland sites could mostly be explained by energy availability. Forest evaporation can mainly be explained by water availability, urban evaporation by water availability and exchange efficiency, and open water evaporation can almost entirely be explained by exchange efficiency. We found that the sensible heat flux is less sensitive to land cover type. This demonstrates that the land-atmosphere interface plays an active role in the shedding of sensible heat. Our results contribute to a better understanding of the dynamics of evaporation over different land cover types and may help to optimize, and potentially simplify, models to predict evaporation.

**Plain Language Summary** At the land surface solar energy is divided into evaporation and warming of the air (sensible heat). Land cover controls the land-atmosphere exchange of water and energy through this division. Over the past years, there is a growing interest in how land use management can be used to optimize local water and climate services by influencing this division. However, this requires a good understanding of the drivers of evaporation and sensible heat. In this study, we aim to study the role of land cover type on the drivers of daily and midday evaporation and sensible heat during warm seasons. Therefore, we used fields observations, the eddy covariance technique, from 19 sites in the Netherlands covering six different land cover types in a regression analysis. The drivers are expressed along three axes: energy availability, water availability and exchange efficiency. We found that evaporation dynamics from grassland, peatland swamp and cropland sites could mostly be explained by energy availability. Forest evaporation can mainly be explained by water availability, urban evaporation by water availability and exchange efficiency, and open water evaporation can almost entirely be explained by exchange efficiency. We also found that sensible heat fluxes are less sensitive to land cover type.

## 1. Introduction

Partitioning of solar energy at the land surface into latent heat or evaporation and sensible heat is a key process in the climate system, and a main control on the terrestrial part of the hydrological cycle (Seneviratne et al., 2010).

© 2023. The Authors.

This is an open access article under the terms of the [Creative Commons Attribution License](https://creativecommons.org/licenses/by/4.0/), which permits use, distribution and reproduction in any medium, provided the original work is properly cited.

The partitioning is strongly controlled by vegetation and soil moisture, resulting in reduced evaporation during drought due to soil moisture limitation. The associated higher sensible heat fluxes can amplify heatwave temperatures (Miralles et al., 2014, 2019). In a warming climate, it is projected that many regions will face increased water limitation, with important implications for heatwaves and ecosystem functioning (Denissen et al., 2022). Within hydrology, the total evaporation from the vegetated land surface is commonly referred to as evapotranspiration. Since the use of this term has come under scrutiny for various reasons (Miralles et al., 2020; Savenije, 2004), we will simply use “evaporation” in this study to refer to the total flux of water from the (land) surface to the atmosphere. Generally, there is a focus on understanding the dynamics and drivers of evaporation rather than the sensible heat flux when analyzing land surface-atmosphere exchange processes (Brutsaert, 1982). Observations of the sensible heat flux are predominantly made to serve the aim of energy balance closure (Katul & Parlange, 1992; Vercauteren et al., 2009). As a result, the active role of the land surface in driving the sensible heat flux has remained under-explored (Wilson et al., 2002). Over the past years, however, interest in the use of land use management as a tool to optimize not only local water but also local climate services has been growing. In addition to the role of evaporation in controlling water availability, sensible heat fluxes can be used to control near-surface temperature in particular during the warm season when energy balance partitioning at the land surface has the largest impact on atmospheric conditions. So far, however, few studies have investigated the variability of flux partitioning and its drivers in a climatologically homogeneous region such as the low-lying countries of the Rhine-Meuse delta with a temperate marine climate.

Historically, studies on the exchange of water and heat at the land surface were based on theoretical concepts rather than observations. Already in the 12th century, hypotheses were presented in which possible explanations for evaporation were given (Brutsaert, 1982). The integration of experiments and theoretical hypotheses as a scientific approach created opportunities to improve our understanding of the evaporation process. The findings by Dalton (1802), who was able to relate evaporation to wind speed and vapour pressure gradient, formed a crucial step in the development of evaporation theory. More than a century later, Thornthwaite (1948) introduced the concept of potential evapotranspiration (PET), which describes the atmospheric evaporative ability over large uniform surfaces (implying no effects of local advection), in which evaporation rates rise to their maximum depending solely on the climatic setting, thereby assuming unlimited water access. A more elaborate method, which considers additional meteorological input, was developed by Penman (1948). He described potential evaporation (PE) from a wet surface as the sum of a radiation and an aerodynamic term, both expressed in terms of energy. This suggests that these two terms could also compensate each other's effects and could therefore be interchangeable. To simulate PET for vegetated surfaces, Monteith (1965) introduced a surface resistance factor ( $r_s$ ) to represent plant physiological processes in the so-called Penman-Monteith (PM) equation. This resistance is a function of atmospheric variables such as radiation, air temperature and vapour pressure deficit (VPD), but it does not integrate the active response of the vegetation to changes in these atmospheric variables, as was proposed by Jarvis (1976). This dependency of  $r_s$  on atmospheric variables in a coupled biological system makes it challenging to understand the exact role of  $r_s$  on the dynamics of evaporation. In fact,  $r_s$  can compensate for all the processes and mechanisms that are included in the PM equation. The interchangeability between the two PM terms is therefore questionable for biological systems. Furthermore, the bidirectional effect of surface fluxes related to their interaction with the planetary boundary layer (PBL) growth is often neglected. This bidirectional effect refers to the feedback mechanism in which the conditions of the PBL are altered by changes in the surface fluxes which, in turn, affect the surface fluxes (C. M. J. Jacobs & De Bruin, 1992; McNaughton & Spriggs, 1986). Fixed values to describe the PBL conditions, as is for instance the case in the PM model, do not allow to study this effect. Nevertheless, many studies have found the PM equation to correctly describe evaporation rates. Therefore, the physically-oriented PM equation is nowadays the default method to estimate evaporation based on standard meteorological data.

Parallel to the development of the physically-oriented theoretical approaches to approximate evaporation, another branch of studies was emerging, which explored simplifications of these physically-oriented theories. This quest for simplification partly originated from limited data availability. This has led to the development of several simpler models to estimate PET compared to the PM equation. For example, Priestley and Taylor (1972) showed that in a land surface-atmosphere system, in which many feedbacks are present, the evaporation tends to reach an equilibrium. This equilibrium evaporation represents the lower limit of evaporation when the air is saturated and thus the drying power of the air is reduced to zero. This would eliminate the second term of the Penman equation. However, conditions without any advection are rare. Therefore, Priestley and Taylor (1972) added a

constant ( $\alpha$ ) to the first Penman term to account for conditions of minimal advection. Other simplified models were developed for specific regions. For instance, the simple linear temperature- and global radiation-based model of Makkink (1957) has been successfully employed in operational water and drought management in the Netherlands since 1987. Makkink (1957) developed this pragmatic model based on the same principles as Priestley and Taylor (1972), but it was specified to conditions in the Netherlands in an attempt to find a model that only includes meteorological variables that were readily available. If global radiation observations are not available either, the highly empirical temperature-based model developed by Hargreaves (1975) is often chosen. This model can be used at longer temporal scales and it accounts for seasonality by using location-specific extra-terrestrial, that is, top-of-the-atmosphere, radiation data estimated from the solar constant, the solar declination and the time of the year. In the aforementioned examples of simplified evaporation models, not all terms of the PM equation are represented. Recently, Maes et al. (2019) demonstrated using eddy covariance (EC) observations that the more complex approaches such as the PM method perform consistently poorer than simpler approaches at daily timescales. By using this modern flux data set, Maes et al. (2019) support the idea that  $r_s$  is highly dynamic and that it might compensate for many atmospheric feedbacks, rather than being a constant as was originally proposed by Monteith (1965). So where physically-oriented approaches might suffer from over-parametrization, EC observations can provide invaluable insight into the control of both vegetation-related processes and atmospheric feedbacks on water and energy exchange at the land surface.

The gradually increasing availability of observations and new measurement techniques allowed to not only study PET, but it also created a shift to start analysing the role and impact of water limitation on actual evaporation. Initially, observations of evaporation could only be determined indirectly through long-term average discharge ( $Q$ ) measurements, from which systems at the larger temporal and spatial scale could be analysed. This does not allow studying the drivers of evaporation in detail, but it can inform us more on the transition from energy to water limitation within a larger river catchment. Budyko (1974) recognized that the long-term water balance of river catchments has two limiting regimes, namely a regime where evaporation is limited by the available energy and a regime where it is limited by water availability. Whether catchments are closer to one than to the other regime depends on the partitioning of precipitation between evaporation and  $Q$ . The so-called Budyko curve can thus be used to identify how water limitation influences the energy partitioning at relatively large spatial and temporal scales. Besides, the Budyko approach can also be used to explore the effect of vegetation on the surface water balance through its coupling with evaporation and runoff (Gan et al., 2021; Gentile et al., 2012; Williams et al., 2012). Later, more recently developed measurement methods, such as the Bowen ratio method and EC, were used to analyse the effect of water limitation on the reduction of evaporation. Brutsaert and Chen (1995) and Williams and Albertson (2004) found a clear relation between soil moisture depletion and the reduction of evaporation rates during experiments performed over a prairie and a savanna landscape, respectively. Studies performed in urban areas using EC and scintillometry measurement techniques found that evaporation in these systems is strongly water limited within days during a drydown and that interception plays an important role in the timing of the total urban evaporation rate (C. Jacobs et al., 2015; Jongen et al., 2022). Originating from the initial focus of the role of energy availability as a driver of evaporation, these more recent observations on the role of water limitation supported the integration of a second dimension to the evaporation limitation concept and to start studying the actual evaporation (Budyko, 1974; Seneviratne et al., 2010). The two-dimensional evaporation limitation concept, where evaporation is constrained by water and energy availability, currently appears to be the commonly used way to present and categorize the drivers of evaporation. The ever-increasing availability of more direct evaporation observations enhances the potential to evaluate the current framework and to continue to study the energy partitioning and drivers of evaporation for different scales, environmental conditions and land cover types.

Over the past decades, advances in sensor and computer technology have turned EC flux measurements from a highly specialized endeavour, used mainly during dedicated field campaigns, into a more routine observation method. Starting from the mid-1990s, this has allowed researchers to routinely measure fluxes of water, energy, and carbon over a range of ecosystems around the world. The FLUXNET initiative (Baldocchi et al., 2001) brought together many of these observations, and has since served as a valuable data set for the study of flux responses to extreme events such as heatwaves and droughts (e.g., Ciais et al. (2005); Teuling et al. (2010)), for the study of land cover impacts on land-atmosphere exchange and atmospheric conditions (e.g., Lee et al. (2011); Lansu et al. (2020); Hoek van Dijke et al. (2020); Xu et al. (2022)), and to study long-term changes in land surface evaporation (e.g., Teuling et al. (2009); Jung et al. (2010)). The location of the flux towers in FLUXNET is however far from random, with a tendency for sites to be located in carbon-rich ecosystems in richer countries,

and less so in dryland ecosystems or for instance in cities. The FLUXNET database is not a comprehensive archive of EC observations either. In many regions, the Netherlands being a good example, only a small minority of the EC sites contributes to the FLUXNET database. In conclusion, while the abundance of EC observations that became available through FLUXNET has provided a tremendous opportunity for global and continental analysis on the drivers of land-atmosphere exchange over different climate zones, the current number of sites is insufficient to study variability of evaporation at the regional scale, and over all land cover types that make up real-world landscapes.

We aim to study the drivers of turbulent exchange over land cover types that are less or not represented in FLUXNET. Results from case studies where other land cover types, such as urban areas, peatland swamps and inland water bodies, are analysed indicate that our knowledge on the drivers of evaporation and the role of land cover type can be further increased. As mentioned earlier, urban areas can be considered water-limited systems. Linked to the vast impervious surfaces in urban areas, it is shown that evaporation in cities is closely linked to precipitation events, or more specifically to the time since precipitation (C. Jacobs et al., 2015; Jongen et al., 2022). During drydowns less water is available for evaporation, which leads to increased air temperatures and thus an increased sensible heat flux ( $H$ ). Van der Velde et al. (2013) showed that peatland swamps use significantly less energy and water for evaporation compared to open water, thereby maintaining or even creating new peatland swamps. The reduced evaporation from peatland swamps compared to open water, could potentially be related to the stronger stomatal control and a lower decoupling factor (Jarvis & McNaughton, 1986) as a result of the higher surface roughness caused by the vegetation. Furthermore, the lower albedo and the reduced air exchange as a result of stable and moist air created in between the peatland swamp vegetation can also contribute to reduced evaporation. Based on regression analysis daily open water evaporation from inland water bodies was found to be dominantly transport-limited and could be explained by a combination of wind speed and a vapour pressure gradient (Granger & Hedstrom, 2011; Jansen et al., 2022). Similarly, Lobos-Roco et al. (2021) found that transport in addition to radiative energy are the principle components to explain the dynamics of evaporation for a saline lake in the Atacama desert. This transport mechanism, consisting of wind speed and a vapour pressure gradient, could be considered a mechanical energy term, similar to the aerodynamic term in the PM equation. However, it can also be looked upon as an exchange efficiency term that controls the exchange processes of energy and water between the land surface and the atmosphere, in which  $r_s$  with its biological controls is eliminated. This exchange efficiency can be weaker or stronger and with that it can explain part of the variance of evaporation. This suggests that the exchange efficiency can be seen as a third dimension, next to energy availability and water availability, to explain evaporation dynamics over different land cover types.

One way to better understand the complexity of turbulent exchange over different systems is by comparing sites of various land cover types located within the same region and climatic setting. By including EC sites beyond the FLUXNET database, we can increase the density of EC sites within a region and thus improve the representation of different land cover such as wetlands and urban areas with respect to FLUXNET. The multitude of EC measurements conducted over different land cover types in the Netherlands provides the opportunity to perform a direct comparison of drivers of evaporation over land cover types within the same climatic zone, and largely in the absence of orographic differences. The landscape of the Netherlands is almost completely anthropogenically managed, resulting in a mosaic of urban areas, forest, grassland, agriculture, peatland swamps and open water areas, all in close proximity. Long-term EC measurements of latent and sensible heat exchange by eddy covariance have been performed over the grassland areas Cabauw, Veenkampen and Horstermeer (Bosveld et al., 2020; Hendriks et al., 2007; A. F. G. Jacobs et al., 2010). The coniferous forests of Loobos (Dolman et al., 1998; Moors, 2012) and Speulderbos (Bosveld & Bouten, 2001; Cisneros Vaca et al., 2018) both have a long history of EC measurements as well, while in Oostwaard there was a short measurement campaign over a willow forest (Elbers et al., 2009). In the past, various croplands have been studied, that is, locations Dijkgraaf, Langerak, Lutjewad, Molenweg, Vredepeel and Zeewolde (Elbers et al., 2009; Moors et al., 2012). More recently, open water evaporation from lake IJssel was studied at two locations: Stavoren and Trintelhaven (Jansen et al., 2022). Furthermore, evaporation in the urban areas of Arnhem and Amsterdam has been studied (C. Jacobs et al., 2015; Jongen et al., 2022; Steeneveld et al., 2020), and in recent years measurement campaigns over the peatland swamps Onlanden, Camphuys and Zegveld have been performed (Buzacott et al., 2022; Kruijt et al., 2020). Additional evaporation observations in The Netherlands have been made based on other techniques, including lysimeters (Teuling, 2018; Voortman et al., 2015), scintillometry (C. Jacobs et al., 2015; Leijnse et al., 2007; Meijninger et al., 2002; Steeneveld et al., 2011), Bowen ratio method (Moors, 2012) and distributed temperature





**Figure 1.** Map of the study area, including the location and land cover type of the measurement sites and the topography of the Netherlands in meters above surface level. The dots on the map represent the locations of the flux tower observations, where the colors indicate the land cover type.

sensing (Schilperoort et al., 2018). However, these methods are either unable to resolve diurnal or even day-to-day variability, or they do not (currently) allow for a comparison between different land cover types. Therefore, EC measurements are currently the best basis for a synthesis of the drivers of evaporation dynamics over different land cover types.

In this study, we aim to compare the external drivers of daily and midday evaporation, expressed in terms of energy, that is, the latent heat flux ( $LE$ ), and sensible heat flux over different land cover types within a climatic zone during the warm season. As a case, we will use EC observations obtained in the Netherlands (i.e., temperate marine climate) over 19 different forest, grassland, urban area, open water, cropland and peatland swamp sites (see Figure 1). These include sites that are part of FLUXNET, but also sites outside that network. This study provides a first synthesis presenting the drivers of observed evaporation dynamics over complex landscapes, which we will express as a three-dimensional framework in which evaporation is found to be limited by either energy availability, water availability or exchange efficiency depending on land cover.

## 2. Data and Methods

### 2.1. Measurement Sites

In this study we analyzed historical measurements of latent heat flux, sensible heat flux and auxiliary meteorological observations from EC flux towers at 19 different sites in the Netherlands, covering six land cover types within

the same temperate marine climate zone. Figure 1 provides an overview of the study region with (a) the location of the flux tower sites and (b) the topographical setting. The Netherlands is a river delta located in north-western Europe and is bordered in the west and north by the North Sea. The Netherlands has a warm temperate humid climate with prevailing south-westerly winds, a long-term average yearly temperature of 10.5°C, precipitation sum of 855 mm and evaporation of 581 mm (KNMI, 2022). Orographic differences are almost absent, with mostly some topography in the very south of the country of which the highest point reaches 322 m above NAP (Normaal Amsterdams Peil, the local sea level reference). More than a quarter of the country is situated below sea level (De Vries, 2007). In the low-lying areas with mostly clay or peat soils groundwater levels are shallow, ranging from two m deep to a few centimeters or less. In the higher ice-pushed ridge areas in the middle, east and the far south of the country the groundwater levels are deeper (up to 20 m deep) but also highly spatially varying (TNO, 2022).

Table 1 provides an overview of all the sites including the land cover classification, period over which measurements were performed, climatological yearly means of air temperature and precipitation, and the key references of each measurement site. The 19 sites were selected based on measurement method (i.e., eddy covariance), data availability of latent heat fluxes and auxiliary meteorological observations, and the requirement of a minimum length of the data record of one warm season (MJJA). The majority of the sites have been operated on a campaign basis for only a relatively short period of one or 2 years, but there are also sites where a long-term measurement effort has been made or is still continued, such as locations Cabauw (grass), Veenkampen (grass), Horstermeer (grass), Loobos (forest), Speulderbos (forest), and Arnhem (urban). The sites Horstermeer and Loobos are part of the FLUXNET database. Besides the sites listed in Table 1, evaporation has been measured at other sites as well using EC, however we have not been able to obtain these data (see Table A1 for an overview of these sites).

Six land cover types are considered in this study, namely: grass (GR), forest (FO), urban (UR), open water (WA), crop (CR) and peatland swamp (PS). The different crops included in this study are maize, wheat, potato and beet (see Table 1). Peatland swamps are vegetated peat areas covered with reed-like vegetation (among others: *Phragmites* spp, *Typha* spp) which are inundated year-round with a shallow standing water level of a few centimetres. This differs from open water bodies, which do not have a significant vegetation cover and typically have deeper water levels. Peatland swamps also differ from grasslands on peat soils in terms of groundwater levels. The various land cover types studied have distinct surface properties that impact the land-atmosphere interaction. The aerodynamic roughness length for the surfaces under study likely ranges from 0.0 m for open water to 0.5 m for coniferous and mixed forests (Floors et al., 2018). The aerodynamic roughness in urban areas is even higher and depends on the urban structure and the dominance of buildings and vegetation (Kent et al., 2017). The albedo also varies considerably. While albedo is time dependent due to changes in vegetation cover, soil moisture and solar altitude, values likely range from 0.05 for open water to 0.3 for grasslands and urban areas (Moene & van Dam, 2014).

## 2.2. Data Processing

All turbulent flux data used in this study were measured with the EC technique, which is considered one of the most direct methods for quantifying turbulent heat fluxes. This technique is based on simultaneous measurements of the vertical wind speed and gas concentration (including water vapor) and temperature measurements. From this the heat fluxes can be derived as the covariance of the vertical wind speed and specific humidity (latent heat flux) and the covariance of the vertical wind speed and temperature (sensible heat flux). While the largely flat terrain in the Netherlands is ideal for applying the EC method, we cannot rule out that advection may play a role at some sites, potentially affecting the resulting fluxes. Raw fluxes were quality-controlled and processed by the individual researchers responsible for their site, respecting and complying with the generally accepted procedures (Aubinet et al., 2012). The data processing of the FLUXNET sites Horstermeer and Loobos naturally followed the required processing pipeline as given by FLUXNET. Fluxes were provided at 30-min or hourly averaging intervals with accompanying quality flags for the heat fluxes. Since we are interested in the process of the turbulent fluxes we chose to only use the best quality data, which means quality flags 1, 2 and 3 in case of the 9 quality flag system of Foken et al. (2004), and quality flag 0 in case of the 0-1-2 system of Mauder and Foken (2004). The use of EC in urban areas is known to be especially challenging (Feigenwinter et al., 2012). Therefore, an exception was made for Amsterdam where also flag 1, based on the system of Mauder and Foken (2004), was allowed because otherwise no data would be left for further analysis. Data of all sites are given in UTC+1.

**Table 1**

*Site Characteristics, Including Key References and Climatological Yearly Means of Air Temperature and Precipitation Based on the Nearest Automatic Meteorological KNMI Station*

Measurement site	Code	Land cover	Location (lat/lon)	Period (used in this study)	Avg. T (°C)	Avg. P (mm)	Energy balance <sup>a</sup>	Key references
Cabauw	GR1	Grass	51.970/4.926	2003–2020	10.4	770	0.85	Beljaars and Bosveld (1997) and Bosveld et al. (2020)
Veenkampen	GR2	Grass	51.981/5.620	2014–2021	10.1	868	0.81	A. F. G. Jacobs et al. (2003, 2010)
Horstermeer	GR3	Grass	52.240/5.071	2004–2011	10.5	855	0.78	C. M. J. Jacobs et al. (2007) and Hendriks et al. (2007)
Loobos	FO1	Forest	52.167/5.744	2003–2018	10.1	868	0.74	Dolman et al. (2002), Elbers et al. (2011), and Moors (2012)
Oostwaard	FO2	Forest	52.832/4.909	2008	10.5	787	0.88	Elbers et al. (2009)
Speulderbos	FO3	Forest	52.251/5.690	2015 and 2020	10.1	868	0.94	Cisneros Vaca et al. (2018), Schilperoort et al. (2018)
Stavoren	WA1	Open water	52.886/5.355	2019–2020	10.2	755	0.61	Jansen et al. (2022)
Trintelhaven	WA2	Open water	52.634/5.417	2019–2020	10.2	824	0.81	Jansen et al. (2022)
Arnhem	UR1	Urban	51.985/5.918	2012–2016	10.1	868	0.99	C. Jacobs et al. (2015)
Amsterdam	UR2	Urban	52.367/4.893	2018–2020	10.7	850	1.23	Steenveld et al. (2020)
Dijkgraaf	CR1	Crop (maize)	51.992/5.646	2007	10.1	868	0.89	Elbers et al. (2009) and Moors et al. (2012)
Langerak	CR2	Crop (maize)	51.954/4.903	2005	10.7	770	0.77	Elbers et al. (2009) and Moors et al. (2012)
Lutjewad	CR3	Crop (wheat)	53.399/6.356	2006	9.9	829	0.84	Van der Laan (2010)
Molenweg	CR4	Crop (potato)	51.65/4.639	2005	10.6	799	0.25	Elbers et al. (2009) and Moors et al. (2012)
Vredepeel	CR5	Crop (beet)	51.532/5.844	2006	10.5	739	0.81	Elbers et al. (2009) and Moors et al. (2012)
Zeewolde	CR6	Crop (maize)	52.335/5.373	2008	10.2	824	0.98	Moors et al. (2012)
Onlanden	PS1	Peatland swamp	53.177/6.524	2020	9.8	805	0.84	Kruijt et al. (2020)
Camphuys	PS2	Peatland swamp	53.155/6.580	2020	9.8	805	0.80	Kruijt et al. (2020)
Zegveld	PS3	Peatland swamp	52.139/4.839	2020–2021	10.4	770	1.34	Buzacott et al. (2022)

<sup>a</sup>Energy balance here defined as the average of the sum of  $LE$  and  $H$  divided by  $R_n$  based on hourly data.



From this processed data set, only the warm season was selected for further analysis. Here we defined the warm season as the 4 months with the highest incoming short-wave radiation, that is, May–August. Hereafter, the terms warm season and year are used interchangeably, but we always refer to the months May–August, if not stated otherwise. In case of Stavoren, Trintelhaven and Lutjewad, wind direction was employed as an additional selection criterion to ensure representation of the aimed land cover type. Furthermore, the analysis was performed on two timescales, namely daily and midday. Midday hours were taken as 11 a.m.–3 p.m. UTC+1. This period is considered long enough to reduce the noise of half-hourly fluxes from the actual signal. Studying the midday evaporation provides the opportunity to study the difference in land-atmosphere coupling over the various land cover types, as well as for interpreting snap shots from satellite overpasses, while the daily timescale is commonly used in water resources management modeling.

For each site the following variables were used to study the drivers of evaporation: latent heat flux, global radiation ( $K_{in}$ ), net radiation ( $R_n$ ), air temperature ( $T_{air}$ ), wind speed ( $u$ ), vapor pressure deficit (VPD), precipitation ( $P$ ) and soil moisture (SM). Soil moisture data for all sites originate from the ERA5-Land reanalysis data set, which is based on the land component of the ECMWF ERA5 climate reanalysis (Muñoz Sabater, 2021). It is a gridded global data set with a spatial resolution of  $0.1^\circ \times 0.1^\circ$  and an hourly temporal resolution. Soil moisture from the first and shallowest layer between 0 and 7 cm was used. A comparison of the ERA5-Land data set to in situ measurements of 5 cm for sites in Europe showed that the standard deviation of the difference between the ERA5-Land data set and the in situ observations is approximately  $0.05 \text{ m}^3 \text{ m}^{-3}$  and the bias approximately  $0.06 \text{ m}^3 \text{ m}^{-3}$  (Muñoz Sabater, 2021). The majority of the other meteorological variables was measured at the site. However, in some cases precipitation (Stavoren, Trintelhaven, Amsterdam, Speulderbos) and radiation data (Stavoren, Trintelhaven) were not available. In those cases data from the nearest automatic meteorological station operated by the Royal Netherlands Meteorological Institute (KNMI) were used. Similarly, if one of the variables was missing for more than 60% of the time, with latent heat flux as reference, data from the nearest station were used to fill the gaps using linear regression. In case of small gaps of at most one hour, the gap was linearly interpolated. Daily averages were only calculated if valid data were available for at least 70% of the time.

### 2.3. Regression Analysis

A regression analysis with nine input variables was performed to try to explain the dynamics of evaporation for each measurement site. By using a regression method we draw conclusions that are informed by the data instead of implementing process-based assumptions. The nine potential driving variables included in the analysis are the following:

- Energy availability: global radiation, net radiation and air temperature.
- Water availability: soil moisture, hours since precipitation (HSP), cumulative precipitation over 3 days (Prec3, characteristic for urban response times (C. Jacobs et al., 2015; Jongen et al., 2022)) and cumulative precipitation over 10 days (Prec10, characteristic for rootzone responses (Teuling et al., 2006)).
- Exchange efficiency: wind speed and vapor pressure deficit.

Here, air temperature is included as part of the energy availability category since it is assumed to indicate the heat available for evaporation to occur, rather than as a transport mechanism. To explain the dynamics of evaporation and sensible heat flux at relatively short temporal scales, that is, daily and midday, requires environmental input variables which are dynamic at a similar scale. Hence, we argue that vegetation factors like NDVI and LAI would not have a large explanatory power at these relatively short time scales. Furthermore, there is a spatial scale issue in terms of footprint when using these satellite-based vegetation indices. Hoek van Dijke et al. (2019) showed that the correlation between these vegetation indices and evaporation is not constant over time. Additionally, the strongest correlation between these vegetation indices and evaporation has been found in studies that encompass large spatial scales covering multiple land cover types. Therefore, care should be taken to use NDVI and LAI to explain evaporation at small spatial scale, for example, the flux tower footprint scale.

The “all subset selection” regression method was used in this study because this method is suitable for analysing large data sets in which it is attempted to explain the dynamics of a dependent variable, here evaporation, with relatively few independent variables (Kutner et al., 2005). Other regression techniques such as Lasso regression or stepwise regression methods would typically be used when there are relatively many input variables with respect to the number of data points. In our case, having large data sets with relatively few input variables it is

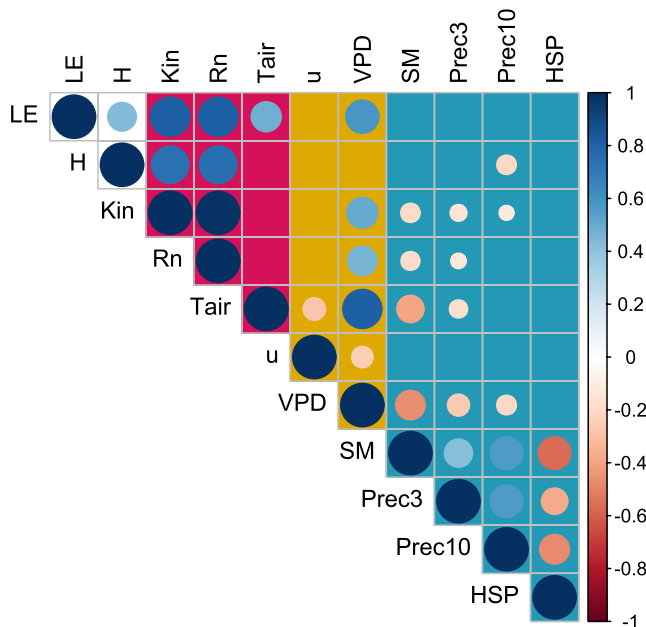


**Figure 2.** Correlation between observed latent heat flux, sensible heat flux and meteorological variables for site GR1 (i.e., Cabauw) at the midday timescale. The size and color of the circles both refer to the correlation strength and sign. Circles are only provided for significant correlations. The background color indicates the grouping of the variables, where pink relates to energy availability, yellow relates to exchange efficiency, and blue relates to water availability.

worth examining all possible combinations from the set of independent variables (i.e., with  $n$  independent variables there are  $2^n$  possible combinations).

For this analysis all input variables were normalized to range between 0 and 100. Furthermore, the regression method requires all variables to be available for each timestep. In case of a missing value, the timestep is removed from the data set. Additionally, temporal independence of each input variable is required. Although we are using time series of environmental variables autocorrelation analysis showed that the temporal dependence in the data is not strong. Apparently the memory of the system is too small to have a large time dependency. To reduce the temporal dependency that is still present, we sampled every other day and used that as a training data set. This way, the autocorrelation falls below the limit of 0.4 within 2 lags for all input variables, except for SM. To eliminate multicollinearity within the model one of the predicting variables would be removed from the subset selection method if it had a higher cross-correlation than 0.7 with other variables. For all sites, high correlations were found between global radiation and net radiation (see Figure 2 for site GR1 as an example). Therefore, the analysis was continued without net radiation as a potential predictor.

Based on the remaining predictors all possible (multiple) linear regression models are identified of which the form is prescribed as:

$$Y = \beta_0 + \beta_1 X_1 + \beta_2 X_2 + \dots + \beta_i X_i + \epsilon \quad (1)$$

where  $Y$  is the dependent variable,  $X_i$  the explanatory variable(s),  $\beta_0$  the intercept,  $\beta_i$  the parameter(s), and  $\epsilon$  the error term. We deliberately opted for a simple linear regression model because we proceed from Occam's Razor principle, which states that the most parsimonious explanation is to be preferred over the more complex one to solve a problem. In our case,

we apply this principle in order to end up with a data-driven model that is able to explain the observed latent and sensible heat flux dynamics, while at the same time the model can be easily used in other studies and is comparable in complexity to many other evaporation equations, such as Makkink's equation. This simplicity allows us to present the results of the analysis directly in the three-dimensional framework. From all the potential subsets the best model for each subset size is returned based on objective statistical criteria, which in this study was chosen to be based on Mallow's Cp value and the AIC (Akaike Information Criterion) value (Kutner et al., 2005). These resulting group of best models are ordered by increasing subset size. In the search for the best parsimonious model from these best models, each of different size, the best model was chosen based on the first instance when (a) both the Cp value would be lower than the sum of the total number of predictors (eight in this study:  $K_{in}$ ,  $T_{air}$ , SM, HSP, Prec3, Prec10,  $u$  and VPD) plus one, (b) as well as the difference between the AIC values of the subsequent best models of increasing size would be less than five. Following this procedure, the number of predictors included in each model for the individual measurement sites can vary.

The best regression model found by the subset selection method was tested for Variance Inflation Factors (VIF), which report whether each predictor in the model is statistically significantly contributing to explaining the dynamics of the dependent variable (Kutner et al., 2005). Because the input data was normalized, the resulting model coefficients provide the relative contribution of each predictor in explaining the dynamics of evaporation. The coefficients of the multiple linear regression model predictors were normalized so they sum up to 100. Originating from our aim to express drivers of evaporation in a three-dimensional framework in which evaporation can be limited by energy availability, water availability or exchange efficiency, the input variables are now grouped according to the categories listed above. The variables belonging to each group have been predefined. The coefficients of the model predictors are summed per category, which then provides the information on the relative contribution of that category in explaining the dynamics of evaporation. Note that a total summation of the coefficients of 100 does not mean that the regression model explains 100% of the variance of the evaporation dynamics; rather, it is used to express the relative contribution of the three limitation categories. The regression procedure described is used as a data analysis technique and is not aimed to have predictive value. Furthermore,

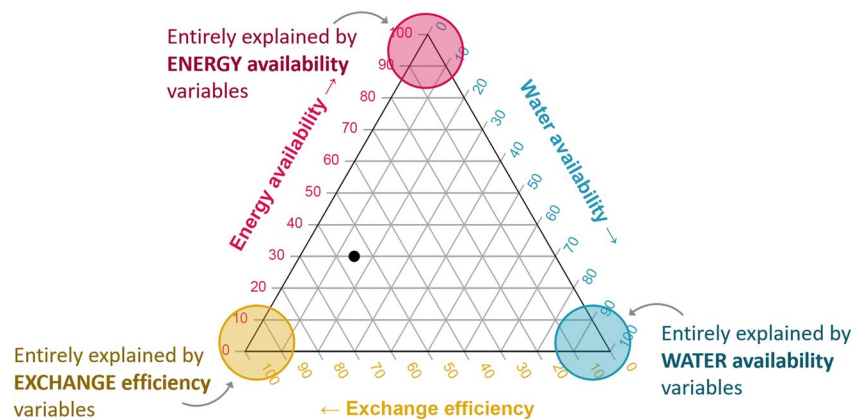


**Figure 3.** Explanation of the triangular plot in which each of the three axes represents one of the limitation categories: energy availability, water availability and exchange efficiency. The position of a measurement site within the triangle (e.g., the black dot) shows the relative contribution of each category in explaining the variance of evaporation for that measurement site. In case of the black dot, the largest portion of the explained variance can be attributed to exchange efficiency (55%), while 30% of the explained variance can be attributed to energy availability and 15% to water availability. If a measurement site ends up in one of the corners of the triangle, it means that all variance explained by the regression model can be attributed to the corresponding category.

since the input data was normalized, the resulting regression models cannot directly be used as predictive models for other sites with potentially different ranges in the input variables. The whole regression analysis procedure was performed for the sensible heat flux as the dependent variable as well, using the same categories of independent variables to explain its dynamics.

Using this regression analysis we were able to study the relative contribution of each of the three groups of variables in explaining the variance of evaporation for each measurement site. These results are presented using a triangular plot, of which each of the three axes represents a group of variables related to energy availability, water availability and exchange efficiency, respectively (Figure 3). If a site is located in one of the far corners of the triangle, it means that the variance explained by the regression model can be entirely explained by the variables belonging to one category. However, this does not mean that 100% of the variance is explained. Similarly, the position of the black dot in Figure 3 indicates that exchange efficiency contributes for 55% to the explained variance of evaporation for that site, while 30% of the explained variance can be attributed to energy availability and 15% to water availability. The variables which are able to explain a portion of the variance in the output signal, can be called driver, given the assumption that the system is sensitive and the driver itself varies and is not constant. In other words, we assume that if variation in the input signal leads to variation in output signal we can call the input variable a driver. In Table B1 the mean and standard deviation of the input variables for each site is shown.

### 3. Results

#### 3.1. Evaporation Dynamics

A clear distinction is found in the diurnal cycle of the latent heat flux ( $LE$ ) between sites of different land cover types (Figure 4). The figure displays the average diurnal cycle for all individual measurement sites, categorized by their land cover types. Note that only the high quality data was used to compute these averaged diurnal cycles, which potentially creates a bias toward conditions without rain. However, we do not consider this a problem in this study since we are studying correlations rather than trends or total sums of the variables. Furthermore, it only rains during approximately 9% of the hours during the warm season (based on data from site GR1). Additionally, the variation of the input variables, which can be seen as an indicator for the variation in meteorological conditions included in the analyses, is large enough to lead to variation in output signal (see Table B1). Especially open water (Figure 4c) and urban areas (Figure 4d) show a distinctively different diurnal cycle of  $LE$ , which does not follow the radiation cycle as strongly as  $LE$  from other land cover types, but is rather more constant throughout the day. In case of open water evaporation, this effect can be related to the relatively large thermal inertia of

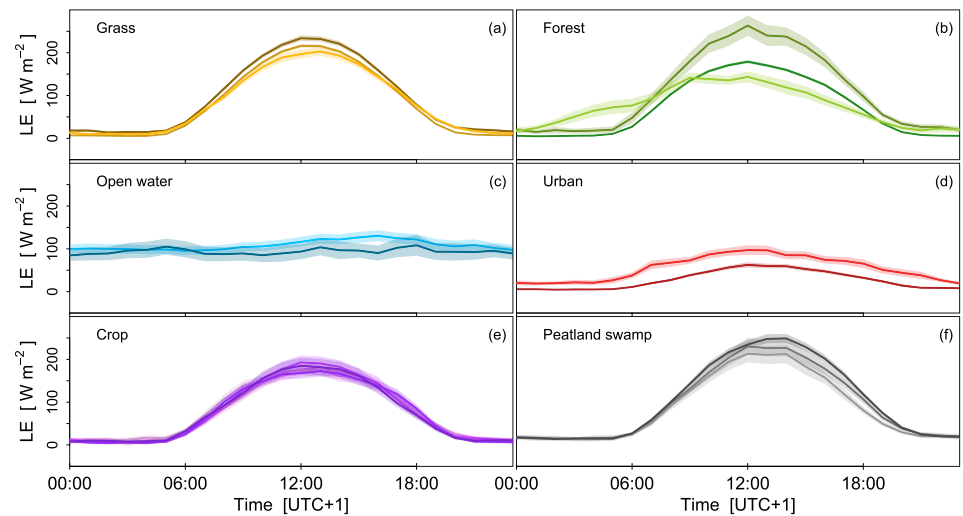


**Figure 4.** Average diurnal cycle of the latent heat flux in the warm season of different land cover types, indicating a difference in sensitivity to environmental drivers. Each colored line represents a measurement site. The uncertainty, here defined as twice the standard error, is presented as the shaded area around the solid lines.

water compared to the vegetated terrestrial surfaces. This large heat capacity also leads to relatively high  $LE$  rates during the night, whereas  $LE$  from other land cover types tend to become zero during the night. At the urban sites, a peak can be found at noon following the radiation cycle, but the amplitude is much smaller compared to the vegetated terrestrial sites. However, the dynamics of sensible heat flux ( $H$ ) shows the reverse behavior (Figure 5), where the peak of urban  $H$  is highest. This is the result of the close relation between  $LE$  and  $H$  through the energy balance. To a first approximation, for closure of the energy balance all available energy not contributing to  $LE$  and heating of the surface must be converted to  $H$ , thereby warming the air.

### 3.2. Drivers of Evaporation

By placing each site within the triangle plot a direct comparison between the sites of different land cover types is possible. Figure 6a shows the results at the daily timescale. In general, the sites are clustered per land cover type. For instance, the open water sites can be found in the lower left corner of the triangle, indicating that exchange

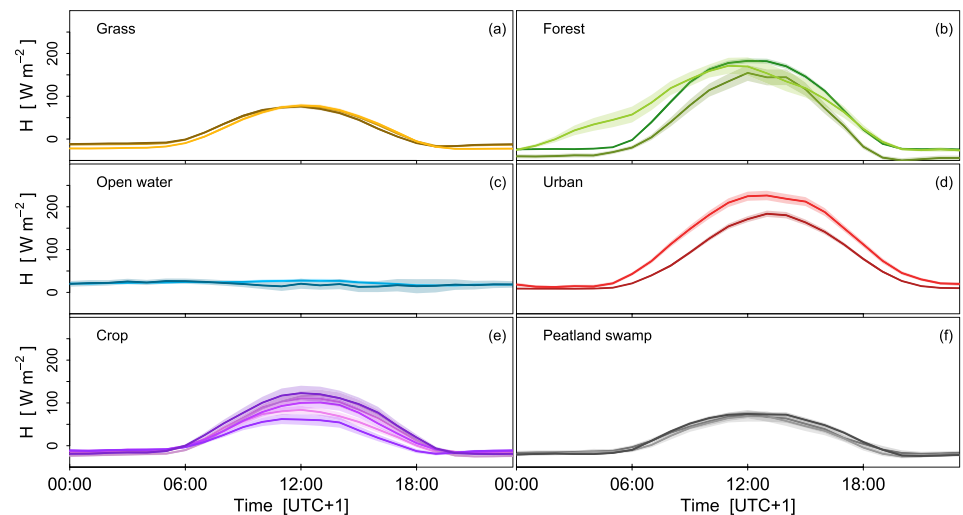


**Figure 5.** Average diurnal cycle of the sensible heat flux in the warm season of different land cover types, indicating a difference in sensitivity to environmental drivers. Each colored line represents a measurement site. The uncertainty, here defined as twice the standard error, is presented as the shaded area around the solid lines.

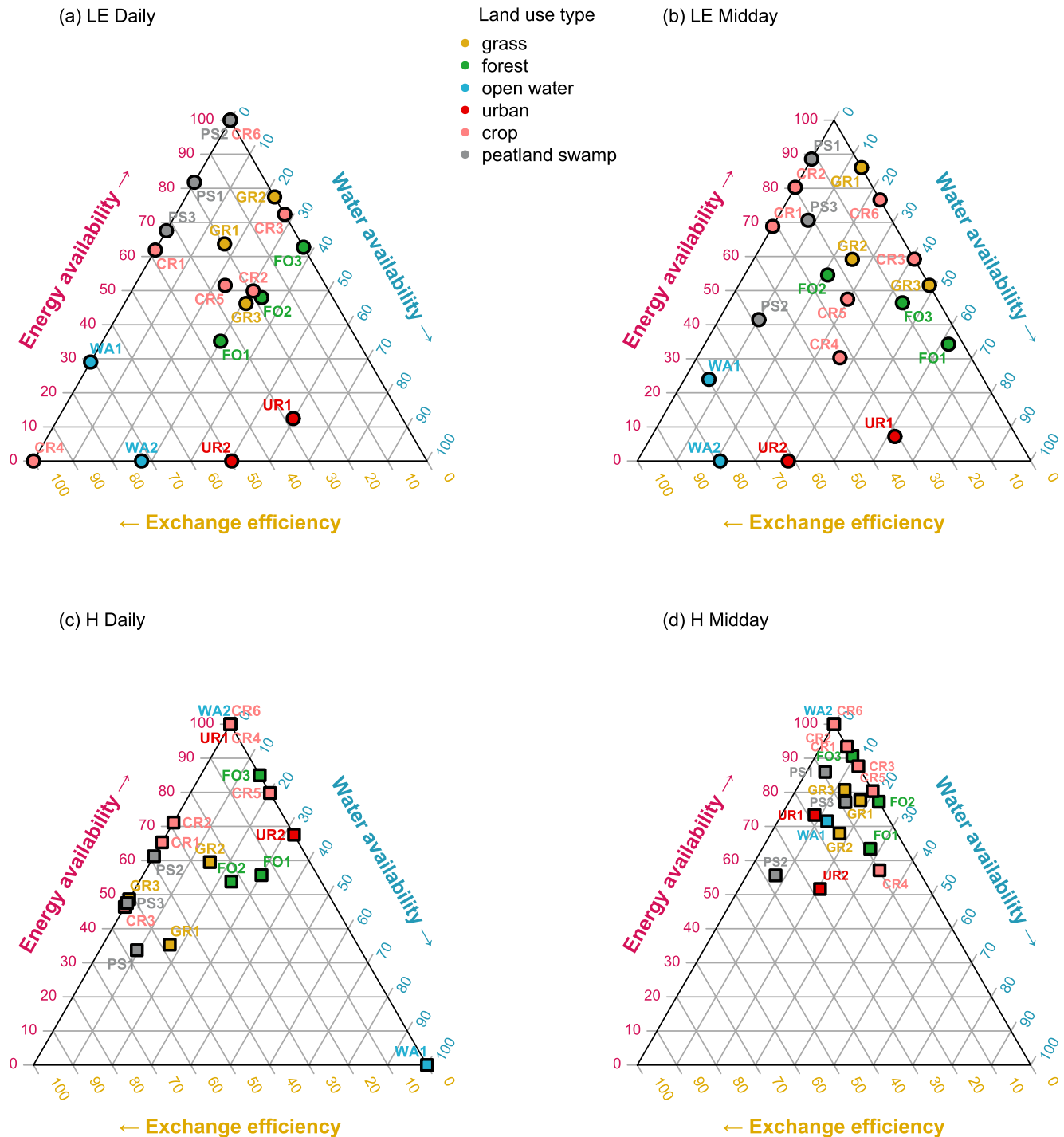


**Figure 6.** A direct comparison of the relative contribution of the variables grouped by energy availability, water availability and exchange efficiency in explaining the dynamics of *LE* (a, b) and *H* (c, d) for sites of different land cover type. Panels (a) and (c) show the results at the daily timescale and panels (b) and (d) for midday hours. The three axes of the triangle each represent a group. For each site the sum of the contributions of the three axes adds to 100%.

efficiency is highly important in explaining evaporation, while energy availability and water availability are contributing less. On a daily timescale this means that if wind speed and/or VPD is low, evaporation will also be less. However, if energy availability is limited, the effect on evaporation will be less strong. The urban areas are found in the lower middle to right part of the triangle. This implies that the variables in the energy availability group are not explaining much of the evaporation dynamics, but rather water availability and exchange efficiency



are important drivers of urban evaporation. The other land cover types, that is, grass, forest, crop and peatland swamp, are mostly situated in the top part of the triangle, indicating the importance of energy availability in driving evaporation. The forest sites tend to be more sensitive to water availability, while for the peatland swamps water is not limiting evaporation at all, as we would expect for inundated vegetated cover. There is one outlier among the crop sites, that is, CR4, which is located in the lower left corner.

In Figure 6b the results of the regression analysis based on midday hours is shown. The positioning of the land cover types is similar as in the analysis based on a daily timescale, although the individual sites shift somewhat. We find that the urban site UR2 moves slightly towards the left, increasing the importance of exchange efficiency at this shorter timescale in the middle of the day at the cost of water availability. The same holds for site WA2. The configuration of the grassland sites changes slightly and a slight shift towards the right can be seen, which means a decrease in the explanatory value of exchange efficiency. A similar behaviour is found for the peatland swamp and crop sites. Also for the forest sites the relative contribution of energy availability to explaining evaporation remains similar at this timescale, but there is some shift on the exchange efficiency and water availability axes. Since the results at both timescales are similar, which might be explained by the fact that largest part of daily evaporation occurs around midday during the warm season, we will focus on the daily timescale in the following analyses.

The results of the regression analysis to explain the driving mechanism of  $H$  differ from that of  $LE$ . The resulting configuration of  $H$  does not resemble that of  $LE$ . Although turbulent eddies are able to transport water vapour and heat, these results imply that the land-atmosphere interface plays an active role in what actually is transported. At the daily timescale almost all sites end up in the top left corner of the triangle, indicating that energy availability is the main driver of  $H$  and that water availability and exchange efficiency are less involved in explaining the dynamics of  $H$ . WA1 is the only site to end up in the lower right corner. Since it is an open water site, it is physically not possible that water availability would be the limiting factor. Therefore, we consider it to be a faulty result from the regression analysis. Some clustering is visible for the land cover types grass, forest and peatland swamp. At the midday timescale the sites end up even more close to each other in the far top corner of the triangle, indicating that  $H$  can mostly be explained by energy availability during midday hours.

The data sets of the sites differ in length and period measured. In Figure 7a the variation between years was explored by plotting the result of the regression analysis for all individual warm seasons ( $N = 1$ , where  $N$  refers to the number of seasons) of one site with a long monitoring period of 18 years, that is, GR1. GR1 was used as the reference site because of its well maintained long data set and land cover, that is, well-watered short grass, which is often used to estimate reference crop evaporation estimation (Allen et al., 1998; McMahon et al., 2013). Note that multiple warm seasons end up in the top corner of the triangle (energy availability = 100, water availability and exchange efficiency = 0), therefore multiple dots overlap. By plotting all individual years separately we can analyse the influence of the conditions of an individual year on the position of the point in the triangle. Similarly, we can identify the position within the triangle when merging two consecutive years, or merging any number of consecutive years. Note that the points are therefore not fully independent of each other. This strategy was chosen over random sampling without replacement, based on the constraints of the data set length. The analysis shows that as more years are included, the points start to converge, reducing the uncertainty, until a single point when

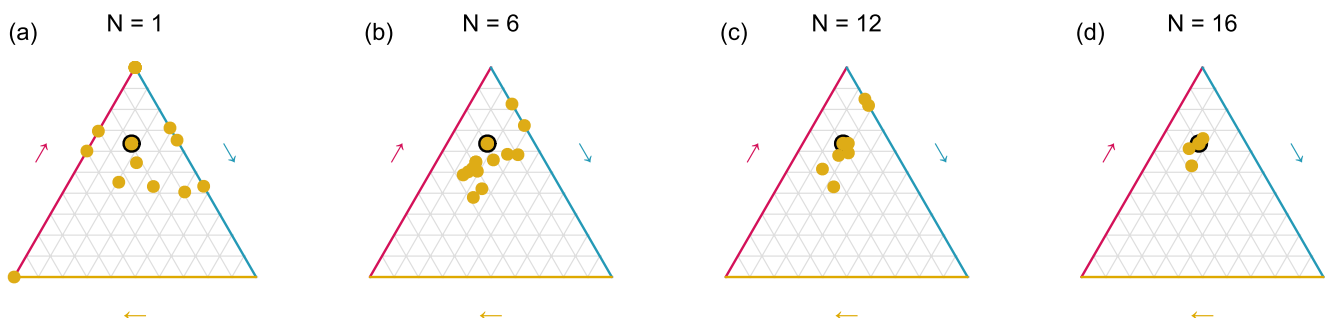


**Figure 7.** Exploration of the effect of inter-annual variability on the positioning within the triangle for the site GR1 at daily timescale. This was used as a reference for identifying the uncertainty ranges for the other sites with shorter monitoring periods. Each yellow dot represents the position based on a moving window of  $N$  aggregated consecutive warm seasons. The black-rimmed yellow dot represents the position when all years are included.

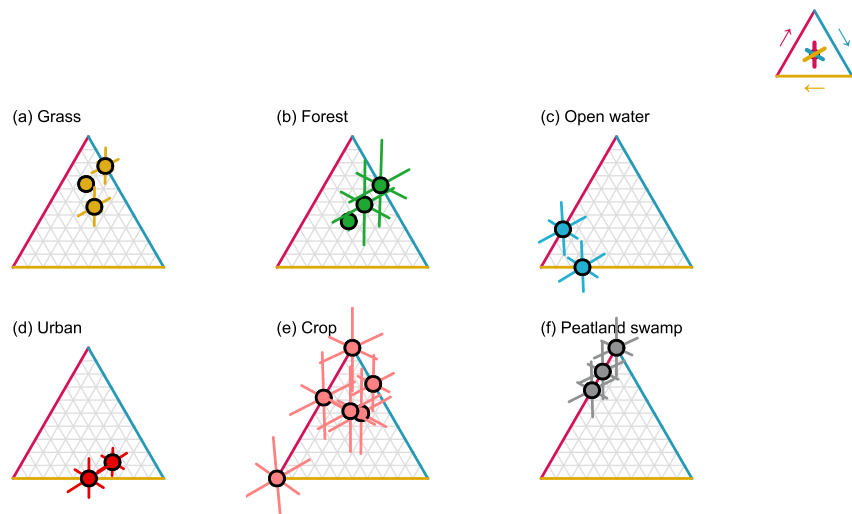


**Figure 8.** Uncertainty analysis per site categorized per land cover type at a daily timescale. The uncertainty bar is the standard deviation calculated for the given number of years of data availability. For these calculations the GR1 data set acted as the reference. The inset on the top-right shows which uncertainty bar belongs to which axis.

all available years within the data set are included (i.e., the points in Figure 6). The results of this analysis are assumed to be suitable as a reference to identify uncertainty ranges for the other sites with shorter monitoring periods. The uncertainty in the three directions of the three axes has been calculated as the standard deviation with the GR1 data set as reference. This has been done for all numbers of years. In that way, the calculated uncertainty ranges can be applied to other data sets where a given number of years of data is available.

In Figure 8 the uncertainty per site is shown categorized per land cover type. The uncertainty bar for each axis is placed perpendicular to the lines belonging to that axis. Note that this is not the same as the direction of the outer lines of the triangle. For instance, the lines belonging to the energy availability axis run horizontally through the triangle, hence the uncertainty bar runs vertically (see inset top-right of Figure 8). Measurement sites with longer time series, for example, FO1, have smaller uncertainty bars, meaning we are more confident in the location within the triangle. For sites with shorter time series, the impact of varying conditions from year to year on the placement within the triangle will likely be larger. Therefore, those sites could be positioned anywhere within the polygon defined by the uncertainty bars. GR1 has no uncertainty bars as this site was used as reference. Given the uncertainty, there is a clear distribution of the land cover types within the triangle.

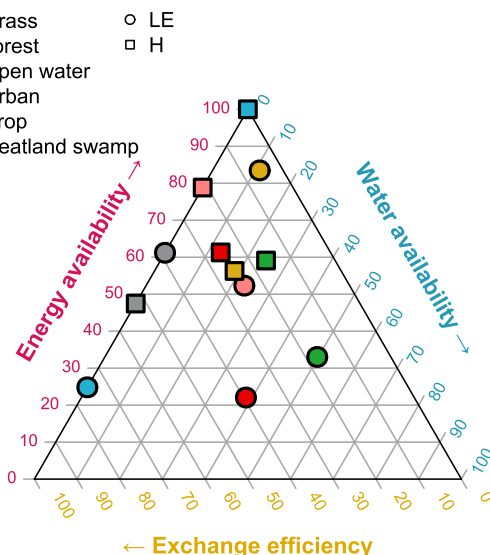


**Figure 9.** Synthesis of the drivers of latent heat flux (circles) and sensible heat flux (squares) per land cover type at a daily timescale. The data of all sites are merged per land cover type.

Figure 9 provides a synthesis of the results per land cover type. Here, the individual site-level is now disregarded and the input data from all sites belonging to a land cover type are merged for the regression analysis. This results in more data and thus less uncertainty of the position of the point. The resulting distinct placement of the six land cover types within the triangle, taking into account the uncertainty, indicates that evaporation drivers are sensitive to land cover type. These drivers can be grouped into three categories, namely energy availability, water availability and exchange efficiency. The terrestrial surfaces covered with short vegetation, that is, grass and crop, are found in the top part of the triangle (energy availability >50%), which indicates the importance of energy availability as the driver of evaporation over these surfaces. Additionally, peatland swamp is found in the same region within the triangle, indicating that the dynamics of evaporation can be explained by similar drivers as to grass and crop, despite the vegetated surface being inundated. The largest relative contribution to explaining the dynamics of evaporation from a forest surface is by water availability (50%), but also energy

availability (33%) is an important driver. Water availability and exchange efficiency are contributing almost the same amount (~40%) in explaining the dynamics of urban evaporation. Open water evaporation is mostly driven by exchange efficiency (75%). The remainder of the dynamics of open water evaporation can be attributed to the energy availability category. The synthesis of the results for  $H$  emphasizes the difference with evaporation. The clustering of all sites, independent of their land cover type, in the top corner indicates that  $H$  is less sensitive to land cover type than evaporation. Interestingly, the difference between the controls for latent and sensible heat fluxes is largest for the land cover types with the smallest potential for biological control (i.e., open water and urban).

The warm season of 2018 was chosen as a case study for a direct comparison of sites under the same meteorological conditions and to study their behavior during a warm and dry season (see Figure 10). Data of three sites, that is, GR1, GR2, and FO1 were available during that year. The summer of 2018 was the hottest in the Netherlands since 1706, with an average temperature of 18.9°C (KNMI, 2018), where the climatological average (i.e., reference period 1991–2020) summer temperature is 17.5°C. Additionally, it was a very dry summer with only 105 mm of precipitation, whilst the average precipitation over a summer is 240 mm. Given these conditions it can be seen that for evaporation site FO1 shifts mainly on the water availability axis relative to its yearly average position. This indicates that the site becomes more sensitive to water availability as a driver of evaporation. The terrain around FO1 is relatively hilly (i.e., ~10 m), with parts where the groundwater is shallower and trees are rooting shallower as well. When the groundwater starts to drop, the trees will soon be unable to reach it, thereby reducing evaporation. In the case of both GR sites the main shift occurs over the energy availability and exchange efficiency axis, while there is hardly any change in the relative contribution of water availability. Both GR1 and GR2 have shallow groundwater levels. Water availability therefore seems to not be limiting evaporation even during a very dry year. For  $H$  the shifts are less strong during this dry year, especially site GR2 hardly shifts. GR1 mainly shifts downward over the energy availability axis, while FO1 shifts upward on the energy availability axis.

#### 4. Discussion

Traditionally, evaporation has been defined in terms of energy- and water-limited regimes (Budyko, 1974; Denissen et al., 2020; Koster et al., 2009; Teuling et al., 2009; Seneviratne et al., 2010). This concept also forms the basis of the widely-used Budyko framework. However, more recent global evaporation studies and studies over inland water bodies have already suggested the existence of a third type of evaporation limitation, namely exchange efficiency-limitation (Granger & Hedstrom, 2011; Jansen et al., 2022; Lobos-Roco et al., 2021; Zhang et al., 2015). Our study, in which a direct comparison of EC measurement sites above different land

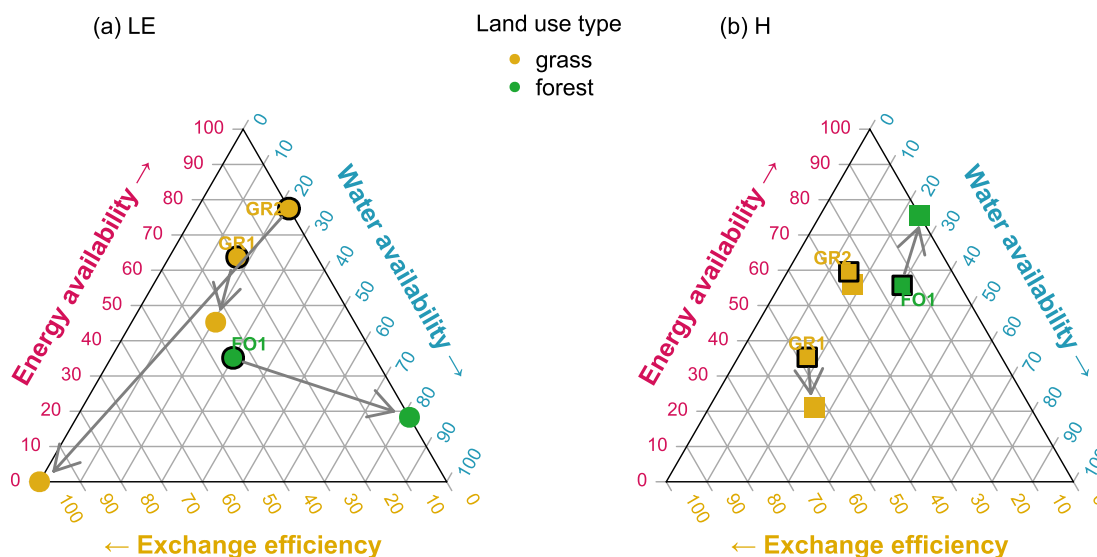


**Figure 10.** Direct comparison of three sites during the drought of 2018 at a daily timescale. The black-rimmed symbols represent the position when all years are included, while the symbols without black represent the warm season 2018. The arrows indicate the shift of the symbol from the yearly average position to the position in 2018. The analysis was performed for both  $LE$  (a) and  $H$  (b).

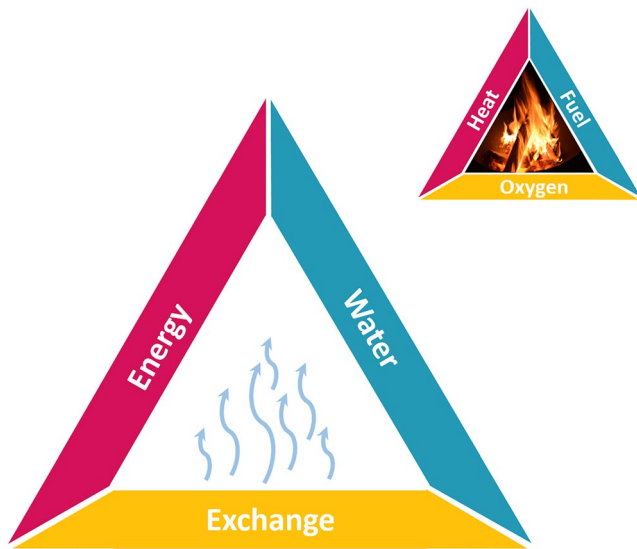


**Figure 11.** Conceptual illustration of the evaporation triangle. This concept is similar to the fire triangle.

cover types was performed, supports the existence of a three-dimensional system. We found that evaporation can be limited by energy availability, water availability or exchange efficiency. Therefore, we argue that the widely adopted two-dimensional system of energy and water-limitation is a simplification of a system which is actually three-dimensional. The idea of a three-dimensional limitation system is not new as we can see the analogy with the concept of a fire triangle where the elements heat, fuel and oxygen determine the conditions under which a fire can exist or not (see Figure 11). If one of these elements is absent, there will be no fire. Similar to the concept of the fire triangle, the position of a site with a certain land cover type in the “evaporation triangle” identifies whether the system is (mainly) limited by energy availability, water availability or exchange efficiency. Interestingly, this study shows that these regimes can co-exist within a relatively small and climatologically homogeneous region. A number of innovative attempts have been made to spatialize land-atmosphere fluxes over complex landscapes at the continental scale (Papale & Valentini, 2003; Xiao et al., 2011) and global scale (Jung et al., 2011) using neural networks. These analyses can for instance be used to study spatial patterns of land-atmosphere fluxes, to derive estimated total fluxes, and to evaluate ecosystem model simulations. However, fluxes from open water and urban areas were not included in these studies. Furthermore, these studies did not aim to identify the drivers of the energy fluxes and to study the difference in drivers of the fluxes over different land use types.

At both the daily and midday timescales, exchange efficiency-limitation was found to be strongest for the inland water body sites. Evaporation from this type of land cover is not directly responding to changes in incoming global energy because of its large heat capacity, it rather responds more directly to the atmospheric demand. There are also other types of land cover that are confronted with exchange efficiency-limitation, albeit to a lesser extent. This is for instance the case for urban environments with fast impermeable surfaces, where the largest fraction of the evaporation dynamics can be explained by water availability (~55%), but the other fraction can mainly be explained by exchange efficiency. The variance in evaporation from peatland swamps at both daily and midday timescales can be explained to a lesser extent by exchange efficiency and to a greater extent by energy availability compared to open water bodies, while both are covered by surface water. This might be explained by the stable and moist layer of air that can be created by the layer of vegetation, thereby reducing the coupling between the water layer and the atmosphere and thus decreasing the importance of exchange efficiency in explaining the evaporation dynamics. At the same time, the vascular vegetation in peatland swamps can still regulate their transpiration through their stomata which can be more related to energy availability. On the contrary, it could also be argued that the increased roughness of the vegetation in peatland swamps compared to open water would lead to a stronger coupling (Jarvis & McNaughton, 1986), which would actually mean a decreased control of evaporation by energy availability and rather a stronger control by changes in stomatal resistance. However, this effect was not shown in this study. The data-driven analysis in this study relies solely on standard meteorological variables, without explicitly considering the active role of vegetation. It can therefore be seen as a statistical analysis of the correlation between evaporation and the meteorological drivers, rather than a causal description of the processes that link the meteorological drivers to evaporation through for instance the role of vegetation.

Based on Figure 6a the relative contribution of the individual variables to explain the dynamics of evaporation was specified in Figure 12. We find that, especially for the sites with short vegetation, energy availability is important in explaining the dynamics of evaporation and in particular global radiation is the main contributor. This is in agreement with other studies over grasslands (Makkink, 1957; Teuling et al., 2010). Our results showed that VPD cannot explain any variance of forest evaporation at sites FO2 and FO3. In the dry year of 2018 our analysis even showed that VPD could not be appointed as driver at any of the three forest sites (see Figure C1), which is in direct contrast to what was found by Moors (2012) and Lansu et al. (2020). They found VPD to be the main driver of forest evaporation during dry and warm summer conditions. For both grassland sites GR1 and GR2 VPD explains a larger portion during the dry year of 2018 compared to when all available years are included in the regression analysis. However, the result for Veenkampen in 2018 is more uncertain as only 18 data points

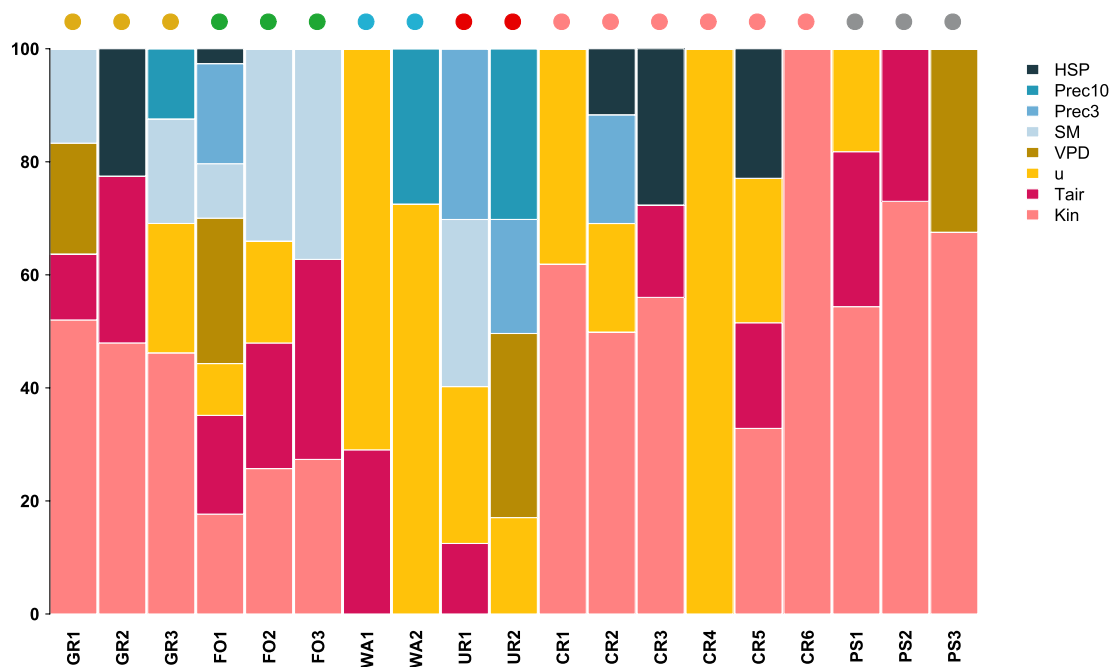


**Figure 12.** Relative contribution of the individual variables in explaining the dynamics of latent heat flux per site at a daily timescale. The colored dots above the bars indicate the land cover type.

were left in the data set. In general, we found a limited role for VPD as driver for evaporation when all years were included. Although there is variability in the input signal of VPD, and thus it potentially could be a driver according to our definition, the limited portion of explained variance by VPD for the different sites may be a limitation of the statistical data approach we used.

As was already noticed in Section 3.2, CR4 seems to be an outlier as it shows that solely wind speed drives evaporation at that site. This outlier position relative to the other crop sites could be due to a lack of data in the data set of CR4 to distinguish between the diurnal cycle of radiation and wind speed. The other crop sites are mostly driven by the energy variables, in particular global radiation, while wind speed is contributing less. A surprising result is found for WA2 where Prec10 partly explains open water evaporation at this site. Since it is a water body, it is impossible from a physical point of view that water availability in any way would be of importance in driving open water evaporation. This indicates a limitation to our data-driven approach combined with the number of data points available to capture and explain the diurnal dynamics. The fact that Prec3 is partly driving evaporation at urban sites is in agreement with what was found in literature (C. Jacobs et al., 2015; Jongen et al., 2022). Our results also show the importance of wind speed and VPD at the urban sites, which could be explained by the response of evaporation to the atmospheric demand when the streets are wet after precipitation. It should be noted that the EC footprint of urban sites reflects the entire urban landscape that exists of a mosaic of different surfaces. Depending on the ratio of impervious and vegetated surfaces a shift in the drivers may be visible, where evaporation dynamics from “greener” urban areas could be expected to behave more similar to evaporation from vegetated surfaces in which energy availability plays a more important role (Loridan & Grimmond, 2012; C. Jacobs et al., 2015).

Our analysis showed that different drivers explain  $H$  compared to  $LE$ . This suggests that the land-atmosphere interface plays an active role in the shedding of  $H$ . Land cover is known to control the land-atmosphere exchange of water and energy through the partitioning of solar energy into latent and sensible heat. Sensible heat is often assumed to follow the latent heat flux because turbulent eddies transport both water vapor and heat, but this is not reflected in our results. Rather, we might argue the opposite to occur if we look at it from a plant physiological point of view:  $LE$  might actually be the resultant of the coping mechanism of how plants deal with heat and moisture stress by regulating their leaf temperature through transpiration (Gates, 1968; Lin et al., 2017). Warm and dry atmospheric conditions lead to higher stomatal resistance, thereby reducing evaporation, which then results into a larger sensible heat flux, which again warms and dries the atmosphere even more (Van Heerwaarden &



Teuling, 2014). However, we cannot explain why the results show substantially different drivers to explain  $H$  compared to  $LE$  for the different land cover types. Thus, our understanding of the drivers of  $H$  and the interplay with the active land surface and vegetation is still not complete.

The warm season months were analyzed in this study. This means that it is not known to what extent these results might be representative for a whole year. The winter season is accompanied by more precipitation and lower temperatures, which might shift the position of sites on the evaporation triangle. Energy availability could become a more prominent limitation for evaporation in that season for the vegetated terrestrial sites. The release of heat during winter that was stored during summer in open water bodies and in urban areas, albeit differently, provides an additional energy source for evaporation. It was not studied if and how this might shift the location of the open water and urban sites within the daily and midday triangles, but it could be argued that energy availability would explain less of the variance of evaporation during winter compared to the vegetated terrestrial sites because more energy is available and thus not limiting evaporation.

In the Netherlands, it is common to have patterns of shade and sunlight projected on the land surface caused by fields of shallow cumulus clouds. This dynamical pattern of direct and diffuse radiation affects the latent and sensible heat fluxes. Vilà-Guerau de Arellano et al. (2020) found that  $LE$  is higher during sunny conditions as compared to cloudy conditions, which can mainly be attributed to the rate of incoming shortwave radiation. This link between incoming shortwave radiation at the surface and presence of clouds is also found by Mol et al. (2023). Furthermore, it was found that  $H$  exhibits a strong correlation with the alterations in radiation resulting from cloud cover, but with a delay of 1–2 min (Vilà-Guerau de Arellano et al., 2020). Given these findings, we argue that the effect of cloud dynamics on the latent and sensible heat fluxes is therefore sufficiently included in our analysis by including incoming shortwave radiation as one of our drivers. Additionally, we think that the effect of clouds on the dynamics of latent and sensible heat fluxes is not a structural issue at the studied spatial (i.e., flux tower footprints in the order of tens to a few hundred meters) and temporal (i.e., daily and midday) scales because cloud cover, cloud properties, and the position of the sun vary over time. Hence, the radiation that reaches the observation sites varies over time even if fields of clouds are present. Therefore, we think that there will be no bias in the results of our analysis as a result of cloud occurrence.

The length of the data sets of the measurement sites included in this study vary. As the uncertainty bars in Figure 8 illustrate, data of multiple warm seasons leads to more confidence on the position of a site within the suggested three-dimensional evaporation limitation diagram. If only one warm season of data is available, the effect of the meteorological conditions will play a larger role on the positioning within the evaporation triangle compared to a multi-year data set. This was for instance visible in the case study of the extremely dry and warm year 2018 (see Figure 10) where a shift of the position within the triangle occurs. Ideally, a multi-year data set and multiple sites per land cover type are used to determine the evaporation regime of that land cover type.

In addition to the simple linear regression models, we tested similar models with interaction and nonlinear terms, as well as a back propagation neural network with two hidden layers (with five and three nodes, respectively). However, the neural network and nonlinear models did not add explanatory power in comparison to the linear regression models. Adding interaction terms to the linear terms did add explanatory power (adjusted  $R^2$  values would raise approximately with 0.05). However, we opted for the parsimonious approach that allowed us to be able to interpret the models and present the result directly in the three-dimensional framework. Despite the uncertainty accompanied with the simple linear regression method used in this study, the additional analyses did not improve the correlations or result into stronger conclusions. Furthermore, we were able to show that the linear regression models perform better at all sites compared to simple linear Makkink's equation, which is the reference evaporation equation in the Netherlands. In particular, a large improvement is found in the case of open water, urban and forest sites (results not shown). This indicates that global radiation ( $K_{in}$ ) is not the most important explanatory variable. However, we are aware that the performance of the developed daily linear regression models is in some cases poor ( $R^2 < 0.60$ ), and thus we can conclude that we still do not capture fully the evaporation dynamics from all the land cover systems. There lies a future challenge. The aim of this paper, however, was to show that land cover controls partly the dynamics of evaporation, and that is what we were able to show in the ternary plots with the resulting clustering of sites per land cover type.

This study was performed in the setting of the Netherlands, which is a country with strong water and land cover management. In general, sufficient water is supplied from upstream catchments to the delta of the Netherlands. The

water is mostly drained as much as possible in this lowland deltaic setting. Other pieces of land are kept artificially wet by inundating the area, which is for example, the case for the peatland swamps. There is a general trend towards retaining more water for periods of drought in the warm season. These artificial settings are the boundary conditions in which this study was performed. The trivial hypothesis in this generally wet lowland country with a humid climate would be that water availability will not be a limiting factor for evaporation from terrestrial vegetated surfaces, but rather that these systems would be energy-limited. However, this study has shown that the water availability axis within the three-dimensional evaporation limitation concept does play a role in the urban, crop, grass and forest sites. Former urban studies have provided a clear indication for this by showing water availability to be a key factor in determining the timing and decay of evaporation rates around a rainfall event (C. Jacobs et al., 2015; Jongen et al., 2022). In forest systems the role of water availability is not trivial because of the role and contribution of interception evaporation during wet conditions to the total daily evaporation (Bosveld & Bouten, 2003; Van Dijk et al., 2015). Through observations it has been shown that transpiration reduces to zero during wet conditions, whereas interception will become the largest contributor to total evaporation during wet conditions and can continue to be high at night (Moors, 2012; Wang-Erlandsson et al., 2014). This in its turn strongly affects the sensible heat flux, which can even become negative and becoming the main energy source for evaporation (De Bruin et al., 1989). The temporal development of the different evaporation fluxes in alternating wet and dry conditions argues for including water availability as a factor to explain the dynamics of total forest evaporation.

Unfortunately, using the EC method to measure turbulent fluxes comes with limitations. One of the best known limitations of the EC method is the problem with a non-closed surface energy balance (SEB). Four topics have been identified to likely contribute to the SEB closure problem, namely instrumental errors, data processing errors, additional sources of energy and sub-mesoscale transport processes (Mauder et al., 2020). It has been shown in several experiments that especially in forests heat storage within the canopy acts as additional energy source or sink, thereby contributing to the SEB closure. In short vegetations this non-closure will be less prominent. Furthermore, the released heat stored in urban areas and open water bodies similarly act as an additional source of energy. The neglected effects and uncertainties of the SEB have been shown to be most significant during the transitions of day and night, which would therefore not be as strong for the daily and midday analyses.

## 5. Conclusions

In this study we analyzed the dynamics of the turbulent heat fluxes of 19 flux tower sites in the Netherlands, covering six different land cover types located within the same climatic zone. The results of the regression analysis performed over the warm season showed that daily and midday evaporation can be mainly limited by energy availability, water availability or exchange efficiency depending on the land cover type. The added value of explicitly including exchange efficiency in explaining the evaporation process, suggests that we could shift from the commonly used two-dimensional system, in which only energy and water-limitation are considered, to a three-dimensional evaporation limitation concept.

Merging of the data per land cover type showed that evaporation from grassland, peatland swamp and cropland can be categorized as mainly energy-limited. Additionally, exchange efficiency-limitation plays a role in describing the dynamics of evaporation from wet peatland swamps, while exchange efficiency and water availability equally contribute to explaining the remainder of crop evaporation dynamics. The dynamics of forest evaporation can be explained for the largest part by water availability. Unexpectedly, we found exchange efficiency, which includes VPD, to contribute to a minor degree only. Open water evaporation is almost entirely explained by exchange efficiency and for the remaining minor part by energy availability. This is in agreement with the findings in previous studies. Urban evaporation is equally explained by water availability and exchange efficiency, while energy availability contributes to a lesser extent.

Given the number of years included in the data sets of individual sites and given the meteorological conditions during that period, the relative contributions of the three limitation categories can shift to some extent. However, the results of the merged data per land cover type provides confidence to the finding that land cover type plays a role in determining the drivers of daily and midday evaporation during the warm season, while  $H$  is found to be less sensitive to land cover type. The results of this study can contribute to a better understanding of the dynamics of evaporation over different land cover types and may help to optimize, and potentially simplify, models to predict evaporation.

## Appendix A: Other Measurement Flux Tower Sites

See Table A1 for the measurement flux tower sites that were not included in this study because the data was not available to us.

**Table A1**  
*Other Measurement Flux Tower Sites in the Netherlands*

Measurement site	Land cover
Langbroekerwetering	Grass
Uden	Grass
Fochteloërveen	Grass
Fleditebos	Forest
Kampina	Forest
Bankenbos	Forest
Utrecht	Urban
Oukoop	Peatland swamp
Stein	Peatland swamp

## Appendix B: Variability of Input Variables

See Table B1 for the mean and standard deviation of the input variables of the measurement sites used in this study.

**Table B1**  
*The Mean and Standard Deviation of the Input Variables of the Measurement Sites*

Measurement site	Kin [ $\text{W m}^{-2}$ ]	Rn [ $\text{W m}^{-2}$ ]	Tair [ $^{\circ}\text{C}$ ]	u [ $\text{m s}^{-1}$ ]	VPD [kPa]	SM [ $\text{m}^3 \text{m}^{-3}$ ]	Prec3 [mm]	Prec10 [mm]	HSP [hr]
Cabauw	220.2 $\pm$ 256.7	116 $\pm$ 175.4	16.6 $\pm$ 4.7	3.7 $\pm$ 2	0.5 $\pm$ 0.5	0.4 $\pm$ 0.1	7 $\pm$ 11.1	23.5 $\pm$ 22.7	148.7 $\pm$ 193.1
Veenkampen	213.1 $\pm$ 255.3	118.2 $\pm$ 175.5	16.9 $\pm$ 5	2.4 $\pm$ 1.5	0.3 $\pm$ 0	0.3 $\pm$ 0.1	7 $\pm$ 9.4	22.7 $\pm$ 18.1	145.7 $\pm$ 183.5
Horstermeer	209.2 $\pm$ 252.4	118.8 $\pm$ 183.1	16.8 $\pm$ 5.1	2.4 $\pm$ 1.3	0.6 $\pm$ 0.6	0.6 $\pm$ 0.1	4.5 $\pm$ 5.9	15.3 $\pm$ 12.8	191.3 $\pm$ 192.2
Loobos	202.2 $\pm$ 248.6	157.5 $\pm$ 223.7	16.2 $\pm$ 4.9	2.1 $\pm$ 1.1	0.5 $\pm$ 0.6	0.2 $\pm$ 0.1	6.3 $\pm$ 9.3	20.4 $\pm$ 19.4	253.6 $\pm$ 406.4
Oostwaard	226.7 $\pm$ 264.6	132 $\pm$ 197.2	16.4 $\pm$ 4.4	1.4 $\pm$ 0.7	0.4 $\pm$ 0.4	0.3 $\pm$ 0.1	2 $\pm$ 2.7	6.5 $\pm$ 5.7	1,025.1 $\pm$ 814.5
Speulderbos	218.7 $\pm$ 269.7	145.3 $\pm$ 234.8	16.1 $\pm$ 5.1	2.9 $\pm$ 1.2	0.4 $\pm$ 0.5	0.1 $\pm$ 0.1	3.6 $\pm$ 5.1	12.3 $\pm$ 10.4	150.4 $\pm$ 129.5
Stavoren	219 $\pm$ 267.3	174.4 $\pm$ 243.3	16.5 $\pm$ 3.8	5.7 $\pm$ 3.1	1 $\pm$ 0.4	–	5.1 $\pm$ 7.4	17.5 $\pm$ 14.7	204.4 $\pm$ 200.5
Trintelhaven	209.5 $\pm$ 261.8	159.5 $\pm$ 240.2	17.8 $\pm$ 4.5	5.3 $\pm$ 2.7	1 $\pm$ 0.4	–	5.1 $\pm$ 7.3	19.5 $\pm$ 15	129.4 $\pm$ 118.5
Arnhem	201 $\pm$ 246.4	129.1 $\pm$ 220.5	17.4 $\pm$ 4.9	2.4 $\pm$ 1.1	0.6 $\pm$ 0.6	0.3 $\pm$ 0.1	4.1 $\pm$ 5.5	13.6 $\pm$ 10.5	231.2 $\pm$ 210.5
Amsterdam	233.7 $\pm$ 272.5	144.3 $\pm$ 224.5	16.2 $\pm$ 4.4	3.9 $\pm$ 1.7	0.4 $\pm$ 0.4	0.5 $\pm$ 0.1	4.5 $\pm$ 7.3	15.2 $\pm$ 15.2	308.3 $\pm$ 388.1
Dijkgraaf	179.1 $\pm$ 227.3	101.7 $\pm$ 166.8	16.8 $\pm$ 4.3	1.4 $\pm$ 0.9	0.5 $\pm$ 0.4	0.3 $\pm$ 0	1 $\pm$ 0.9	3.8 $\pm$ 1.9	1,236.5 $\pm$ 253.6
Langerak	191.1 $\pm$ 232.7	107.1 $\pm$ 170.1	17.8 $\pm$ 4.4	1.5 $\pm$ 0.8	0.5 $\pm$ 0.5	0.4 $\pm$ 0	4.9 $\pm$ 5.2	18 $\pm$ 10.5	169 $\pm$ 169.4
Lutjewad	195.4 $\pm$ 241.3	114.8 $\pm$ 180.4	16.3 $\pm$ 4.4	3.2 $\pm$ 1.7	0.4 $\pm$ 0.4	0.2 $\pm$ 0.1	3.7 $\pm$ 4.6	11.6 $\pm$ 9.5	238.6 $\pm$ 267.1
Molenweg	180 $\pm$ 223	194.7 $\pm$ 195.3	16.7 $\pm$ 3.8	1.7 $\pm$ 1	0.4 $\pm$ 0.4	0.3 $\pm$ 0	3.1 $\pm$ 3.8	10.6 $\pm$ 5.9	203.6 $\pm$ 150.6
Vredepeel	196.3 $\pm$ 242.1	109.9 $\pm$ 174.3	16.8 $\pm$ 5.2	2 $\pm$ 1.3	0.6 $\pm$ 0.6	0.2 $\pm$ 0.1	3.5 $\pm$ 4.6	11 $\pm$ 11.1	304.4 $\pm$ 276.9
Zeewolde	163.2 $\pm$ 210	90.8 $\pm$ 152.8	17.8 $\pm$ 4	3 $\pm$ 0.8	0.4 $\pm$ 0.4	0.2 $\pm$ 0	2.9 $\pm$ 2.7	10.3 $\pm$ 3.5	222.9 $\pm$ 141.1
Onlanden	213.6 $\pm$ 246.6	128.5 $\pm$ 186.3	18.6 $\pm$ 5.6	2.6 $\pm$ 1.3	0.5 $\pm$ 0.6	0.3 $\pm$ 0.1	2.3 $\pm$ 3.4	5.8 $\pm$ 5.7	413.6 $\pm$ 414.1
Camphuys	167.7 $\pm$ 214.8	105.6 $\pm$ 169.2	16.2 $\pm$ 4.9	1.8 $\pm$ 1.3	0.3 $\pm$ 0.3	0.4 $\pm$ 0	1.8 $\pm$ 2.8	6.2 $\pm$ 7.7	552.8 $\pm$ 299.8
Zegveld	301.5 $\pm$ 244.7	184.6 $\pm$ 176.9	17.9 $\pm$ 4.8	1.9 $\pm$ 1.2	0.5 $\pm$ 0.5	0.5 $\pm$ 0.1	6.4 $\pm$ 7.2	20.5 $\pm$ 12.7	143.5 $\pm$ 158.7

## Appendix C: Drivers During the Dry Year 2018

See Figure C1 for the relative contribution of the individual variables in explaining the dynamics of latent heat flux at a daily timescale for the year 2018. The colored dots above the bars indicate the land cover type.

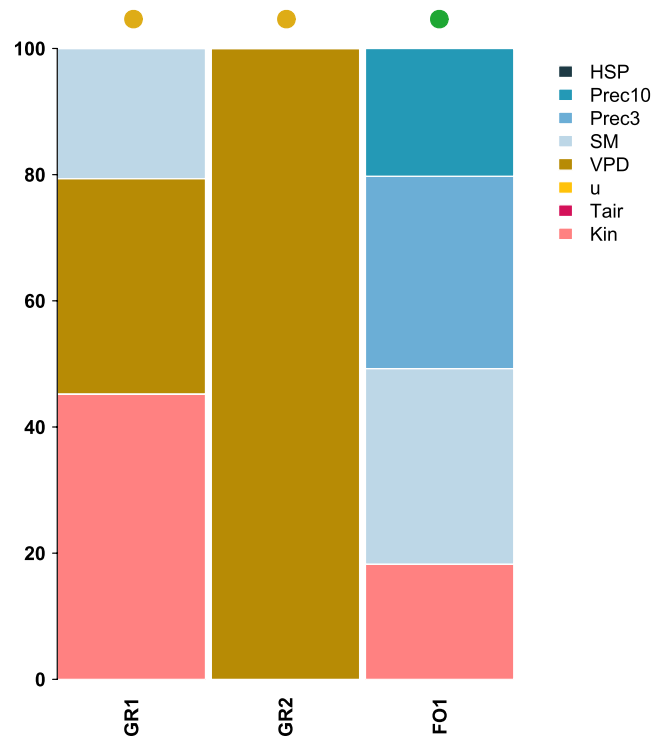


**Figure C1.** Relative contribution of the individual variables in explaining the dynamics of latent heat flux at a daily timescale for the year 2018.

### Acknowledgments

This study is supported by the Dutch Research Council (Nederlandse Organisatie voor Wetenschappelijk Onderzoek (NWO); Grant ALWTW.2016.049). We thank all the Principal Investigators of the eddy covariance flux tower sites used in this study for sharing the data. We thank FLUXNET and European Fluxes Database Cluster for making their data available on the internet. We thank the Dutch Ministry of Agriculture, Nature and Food Quality for supporting the flux sites Onlanden, Camphuys, and Zegveld, and we thank Natuurmonumenten for supporting the flux sites Onlanden and Camphuys as well. GJS acknowledges support from NWO Grant 864.14.007 and AMS-Institute Grant VIR16002 for the Amsterdam flux site. We thank Diego Miralles for providing his valuable feedback on the manuscript. FAJ designed the study supported by AJT, HJJ, and RU. FAJ carried out the study and wrote the manuscript with contributions provided by AJT. All the authors contributed to the interpretation of the results and provided feedback on the manuscript.

### Conflict of Interest

The authors declare no conflicts of interest relevant to this study.

### Data Availability Statement

The warm season daily and midday data of the 19 measurement sites as used in this study can be found in the 4TU data repository (<https://figshare.com/s/8a14ef02b83b5ba984de>). The FLUXNET data are available at <https://fluxnet.org/>. The European Fluxes Database Cluster data are available at <http://www.europe-fluxdata.eu/>. The soil moisture data from the ECMWF ERA5-Land reanalysis data set are available at <https://cds.climate.copernicus.eu/>. Data from Veenkampen site are available at <https://met.wur.nl/veenkampen/data/>. The following people can be contacted for data from the following sites: CvdT for Speulderbos, FAJ for Stavoren and Trintelhaven, CMJJ for Arnhem, GJS for Amsterdam, BGH for Veenkampen, BK for Onlanden and Camphuys, and AB for Zegveld.

### References

- Allen, R. G., Pereira, L. S., Raes, D., & Smith, M. (1998). *Crop evapotranspiration - Guidelines for computing crop water requirements* - FAO *Irrigation and drainage paper* 56. United Nations-Food and Agricultural Organization.
- Aubinet, M., Vesala, T., & Papale, D. (2012). *Eddy covariance: A practical guide to measurement and data analysis*. Springer Science & Business Media.
- Baldocchi, D., Falge, E., Gu, L., Olson, R., Hollinger, D., Running, S., et al. (2001). FLUXNET: A new tool to study the temporal and spatial variability of ecosystem-scale carbon dioxide, water vapor, and energy flux densities. *Bulletin of the American Meteorological Society*, 82(11), 2415–2434. [https://doi.org/10.1175/1520-0477\(2001\)082<2415:FANTTS>2.3.CO;2](https://doi.org/10.1175/1520-0477(2001)082<2415:FANTTS>2.3.CO;2)

- Beljaars, A. C. M., & Bosveld, F. C. (1997). Cabauw data for the validation of land surface parameterization schemes. *Journal of Climate*, 10(6), 1172–1193. [https://doi.org/10.1175/1520-0442\(1997\)010<1172:CDFTVO>2.0.CO;2](https://doi.org/10.1175/1520-0442(1997)010<1172:CDFTVO>2.0.CO;2)
- Bosveld, F. C., Baas, P., Beljaars, A. C. M., Holtslag, A. A. M., de Arellano, J. V.-G., & Van de Wiel, B. J. H. (2020). Fifty years of atmospheric boundary-layer research at cabauw serving weather, air quality and climate. *Boundary-Layer Meteorology*, 177(2), 583–612. <https://doi.org/10.1007/s10546-020-00541-w>
- Bosveld, F. C., & Bouten, W. (2001). Evaluation of transpiration models with observations over a Douglas-fir forest. *Agricultural and Forest Meteorology*, 108(4), 247–264. [https://doi.org/10.1016/S0168-1923\(01\)00251-9](https://doi.org/10.1016/S0168-1923(01)00251-9)
- Bosveld, F. C., & Bouten, W. (2003). Evaluating a model of evaporation and transpiration with observations in a partially wet Douglas-fir forest. *Boundary-Layer Meteorology*, 108(3), 365–396. <https://doi.org/10.1023/A:1024148707239>
- Brutsaert, W. (1982). *Evaporation into the atmosphere: Theory, history and applications*. Springer Netherlands.
- Brutsaert, W., & Chen, D. (1995). Desorption and the two stages of drying of natural tallgrass prairie. *Water Resources Research*, 31(5), 1305–1313. <https://doi.org/10.1029/95WR00323>
- Budyko, M. I. (1974). *Climate and life*. Academic Press.
- Buzacott, A., Mulder, H., van den Berg, M., Kruijt, B., & van der Velde, Y. (2022). Quantifying the contribution of grassland and paludiculture to carbon fluxes from a single eddy covariance tower in a Dutch peatland. In *EGU general assembly 2022* (Vol. EGU22-9978). Copernicus Meetings. <https://doi.org/10.5194/egusphere-egu22-9978>
- Ciais, P., Reichstein, M., Viovy, N., Granier, A., Ogée, J., Allard, V., et al. (2005). Europe-wide reduction in primary productivity caused by the heat and drought in 2003. *Nature*, 437(7058), 529–533. <https://doi.org/10.1038/nature03972>
- Cisneros Vaca, C., van der Tol, C., & Ghimire, C. P. (2018). The influence of long-term changes in canopy structure on rainfall interception loss: A case study in Spuelderbos, The Netherlands. *Hydrology and Earth System Sciences*, 22(7), 3701–3719. <https://doi.org/10.5194/hess-22-3701-2018>
- Dalton, J. (1802). Experimental essays on the constitution of mixed gases: On the force of steam or vapour from water or other liquids in different temperatures, both in a Torricelli vacuum and in air; on evaporation; and on expansion of gases by heat. *Memoirs of the Literary and Philosophical Society of Manchester*, 5, 536–602.
- De Bruin, H. A. R., Jacobs, C. M. J., Jarvis, P. G., McNaughton, K. G., Milford, J., Kohsiek, W., et al. (1989). Forests and regional-scale processes. *Philosophical Transactions of the Royal Society of London B Biological Sciences*, 324(1223), 393–406. <https://doi.org/10.1098/rstb.1989.0054>
- Denissen, J. M. C., Teuling, A., Pitman, A., Koirala, S., Migliavacca, M., Li, W., et al. (2022). Widespread shift from ecosystem energy to water limitation with climate change. *Nature Climate Change*, 12(7), 677–684. <https://doi.org/10.1038/s41558-022-01403-8>
- Denissen, J. M. C., Teuling, A. J., Reichstein, M., & Orth, R. (2020). Critical soil moisture derived from satellite observations over Europe. *Journal of Geophysical Research: Atmospheres*, 125(6), 1–10. <https://doi.org/10.1029/2019JD031672>
- De Vries, J. (2007). Groundwater. In *Geology of The Netherlands* (Ed.), In T. E. Wong, D. A. J. Batjes, & J. de Jager (Eds.), (pp. 295–315). Royal Netherlands Academy of Arts and Sciences.
- Dolman, A. J., Moors, E. J., & Elbers, J. A. (2002). The carbon uptake of a mid latitude pine forest growing on sandy soil. *Agricultural and Forest Meteorology*, 111(3), 157–170. [https://doi.org/10.1016/S0168-1923\(02\)00024-2](https://doi.org/10.1016/S0168-1923(02)00024-2)
- Dolman, A. J., Moors, E. J., Elbers, J. A., & Snijders, W. (1998). Evaporation and surface conductance of three temperate forests in The Netherlands. *Annales des Sciences Forestières*, 55(1–2), 255–270. <https://doi.org/10.1051/forest:19980115>
- Elbers, J. A., Jacobs, C. M. J., Kruijt, B., Jans, W. W. P., & Moors, E. J. (2011). Assessing the uncertainty of estimated annual totals of net ecosystem productivity: A practical approach applied to a mid latitude temperate pine forest. *Agricultural and Forest Meteorology*, 151(12), 1823–1830. <https://doi.org/10.1016/j.agrformet.2011.07.020>
- Elbers, J. A., Moors, E., & Jacobs, C. (2009). *Gemeten actuele verdamping voor twaalf locaties in Nederland* (Tech. Rep. No. Alterra-rapport 1920). Wageningen UR Alterra.
- Feigenwinter, C., Vogt, R., & Christen, A. (2012). Eddy covariance measurements over urban areas. In *Eddy covariance: A practical guide to measurement and data analysis* (pp. 377–397). Springer Science & Business Media.
- Floors, R., Enevoldsen, P., Davis, N., Arnqvist, J., & Dellwik, E. (2018). From lidar scans to roughness maps for wind resource modelling in forested areas. *Wind Energy Science*, 3(1), 353–370. <https://doi.org/10.5194/wes-3-353-2018>
- Foken, T., Gockede, M., Mauder, M., Mahrt, L., Amiro, B., & Munger, W. (2004). Chapter 9 - Post-field data quality control. In *Handbook of micrometeorology* (pp. 181–208). Springer Science + Business Media, Inc.
- Gan, G., Liu, Y., & Sun, G. (2021). Understanding interactions among climate, water, and vegetation with the Budyko framework. *Earth-Science Reviews*, 212, 103451. <https://doi.org/10.1016/j.earscirev.2020.103451>
- Gates, D. M. (1968). Transpiration and leaf temperature. *Annual Review of Plant Physiology*, 19(1), 211–238. <https://doi.org/10.1146/annurev.pp.19.060168.001235>
- Gentine, P., D'Odorico, P., Lintner, B. R., Sivandran, G., & Salvucci, G. (2012). Interdependence of climate, soil, and vegetation as constrained by the Budyko curve. *Geophysical Research Letters*, 39(19), L19404. <https://doi.org/10.1029/2012GL053492>
- Granger, R. J., & Hedstrom, N. (2011). Modelling hourly rates of evaporation from small lakes. *Hydrology and Earth System Sciences*, 15(1), 267–277. <https://doi.org/10.5194/hess-15-267-2011>
- Hargreaves, G. H. (1975). Moisture availability and crop production. *Transactions of the ASAE*, 18(5), 0980–0984. <https://doi.org/10.13031/2013.36722>
- Hendriks, D. M. D., van Huissteden, J., Dolman, A. J., & van der Molen, M. K. (2007). The full greenhouse gas balance of an abandoned peat meadow. *Biogeosciences*, 4(3), 411–424. <https://doi.org/10.5194/bg-4-411-2007>
- Hoek van Dijke, A. J., Mallick, K., Schlerf, M., Machwitz, M., Herold, M., & Teuling, A. J. (2020). Examining the link between vegetation leaf area and land-atmosphere exchange of water, energy, and carbon fluxes using FLUXNET data. *Biogeosciences*, 17(17), 4443–4457. <https://doi.org/10.5194/bg-17-4443-2020>
- Jacobs, A. F. G., Heusinkveld, B. G., & Holtslag, A. A. M. (2003). Carbon dioxide and water vapour flux densities over a grassland area in The Netherlands. *International Journal of Climatology*, 23(13), 1663–1675. <https://doi.org/10.1002/joc.959>
- Jacobs, A. F. G., Heusinkveld, B. G., & Holtslag, A. A. M. (2010). Eighty years of meteorological observations at Wageningen, The Netherlands: Precipitation and evapotranspiration. *International Journal of Climatology*, 30(9), 1315–1321. <https://doi.org/10.1002/joc.1957>
- Jacobs, C., Elbers, J., Broelsma, R., Hartogensis, O., Moors, E., Rodríguez-Carretero Márquez, M. T., & van Hove, B. (2015). Assessment of evaporative water loss from Dutch cities. *Building and Environment*, 83, 27–38. <https://doi.org/10.1016/j.buildenv.2014.07.005>
- Jacobs, C. M. J., & De Bruin, H. A. R. (1992). The sensitivity of regional transpiration to land-surface characteristics: Significance of feedback. *Journal of Climate*, 5(7), 683–698. [https://doi.org/10.1175/1520-0442\(1992\)005<0683:TSORTT>2.0.CO;2](https://doi.org/10.1175/1520-0442(1992)005<0683:TSORTT>2.0.CO;2)
- Jacobs, C. M. J., Jacobs, A. F. G., Bosveld, F. C., Hendriks, D. M. D., Hensen, A., Kroon, P. S., et al. (2007). Variability of annual CO<sub>2</sub> exchange from Dutch grasslands. *Biogeosciences*, 4(5), 803–816. <https://doi.org/10.5194/bg-4-803-2007>



- Jansen, F. A., Uijlenhoet, R., Jacobs, C. M. J., & Teuling, A. J. (2022). Evaporation from a large lowland reservoir – Observed dynamics and drivers during a warm summer. *Hydrology and Earth System Sciences*, 26(11), 2875–2898. <https://doi.org/10.5194/hess-26-2875-2022>
- Jarvis, P. G. (1976). The interpretation of the variations in leaf water potential and stomatal conductance found in canopies in the field. *Philosophical Transactions of the Royal Society of London. Series B, Biological Sciences*, 273(927), 593–610.
- Jarvis, P. G., & McNaughton, K. G. (1986). Stomatal control of transpiration: Scaling up from leaf to region. In A. MacFadyen & E. D. Ford (Eds.), *Advances in ecological research* (Vol. 15, pp. 1–49). Academic Press. [https://doi.org/10.1016/S0065-2504\(08\)60119-1](https://doi.org/10.1016/S0065-2504(08)60119-1)
- Jongen, H., Steeneveld, G.-J., Beringer, J., Christen, A., Chrysoulakis, N., Fortuniak, K., et al. (2022). Urban water storage capacity inferred from observed evapotranspiration recession. *Geophysical Research Letters*, 49(3), 1–11. <https://doi.org/10.1029/2021GL096069>
- Jung, M., Reichstein, M., Ciais, P., Seneviratne, S. I., Sheffield, J., Goulden, M. L., et al. (2010). Recent decline in the global land evapotranspiration trend due to limited moisture supply. *Nature*, 467(7318), 951–954. <https://doi.org/10.1038/nature09396>
- Jung, M., Reichstein, M., Margolis, H. A., Cescatti, A., Richardson, A. D., Arain, M. A., et al. (2011). Global patterns of land-atmosphere fluxes of carbon dioxide, latent heat, and sensible heat derived from eddy covariance, satellite, and meteorological observations. *Journal of Geophysical Research*, 116(G3), G00J07. <https://doi.org/10.1029/2010JG001566>
- Katul, G. G., & Parlange, M. B. (1992). A Penman-Brutsaert Model for wet surface evaporation. *Water Resources Research*, 28(1), 121–126. <https://doi.org/10.1029/91WR02324>
- Kent, C. W., Grimmond, S., & Gatey, D. (2017). Aerodynamic roughness parameters in cities: Inclusion of vegetation. *Journal of Wind Engineering and Industrial Aerodynamics*, 169, 168–176. <https://doi.org/10.1016/j.jweia.2017.07.016>
- KNMI. (2018). KNMI - Zomer 2018 (juni, juli, augustus).
- KNMI. (2022). KNMI - Klimaatviewer.
- Koster, R. D., Schubert, S. D., & Suarez, M. J. (2009). Analyzing the concurrence of meteorological droughts and warm periods, with implications for the determination of evaporative regime. *Journal of Climate*, 22(12), 3331–3341. <https://doi.org/10.1175/2008JCLI2718.1>
- Kruijt, B., Jacobs, C., Berghuis, H., Biermann, J., Letink, R., Jans, W., et al. (2020). Natuurlijke Klimaatbuffers – natte natuur in noord-Nederland.
- Kutner, M. H., Nachtsheim, C. J., Neter, J., & Li, W. (2005). *Applied linear statistical models* (5th ed.). McGraw-Hill Irwin.
- Lansu, E. M., van Heerwaarden, C. C., Stegehuis, A. I., & Teuling, A. J. (2020). Atmospheric aridity and apparent soil moisture drought in European forest during heat waves. *Geophysical Research Letters*, 47(6), 1–8. <https://doi.org/10.1029/2020GL087091>
- Lee, X., Goulden, M. L., Hollinger, D. Y., Barr, A., Black, T. A., Bohrer, G., et al. (2011). Observed increase in local cooling effect of deforestation at higher latitudes. *Nature*, 479(7373), 384–387. <https://doi.org/10.1038/nature10588>
- Leijnse, H., Uijlenhoet, R., & Stricker, J. N. M. (2007). Hydrometeorological application of a microwave link: 1. Evaporation. *Water Resources Research*, 43(4), 1–9. <https://doi.org/10.1029/2006WR004988>
- Lin, H., Chen, Y., Zhang, H., Fu, P., & Fan, Z. (2017). Stronger cooling effects of transpiration and leaf physical traits of plants from a hot dry habitat than from a hot wet habitat. *Functional Ecology*, 31(12), 2202–2211. <https://doi.org/10.1111/1365-2435.12923>
- Lobos-Roco, F., Hartogensis, O., Vilà-Guerau de Arellano, J., de la Fuente, A., Muñoz, R., Rutllant, J., & Suárez, F. (2021). Local evaporation controlled by regional atmospheric circulation in the Altiplano of the Atacama Desert. *Atmospheric Chemistry and Physics*, 21(11), 9125–9150. <https://doi.org/10.5194/acp-21-9125-2021>
- Loridan, T., & Grimmond, C. S. B. (2012). Characterization of energy flux partitioning in urban environments: Links with surface seasonal properties. *Journal of Applied Meteorology and Climatology*, 51(2), 219–241. <https://doi.org/10.1175/JAMC-D-11-038.1>
- Maes, W. H., Gentile, P., Verhoest, N. E. C., & Miralles, D. G. (2019). Potential evaporation at eddy-covariance sites across the globe. *Hydrology and Earth System Sciences*, 23(2), 925–948. <https://doi.org/10.5194/hess-23-925-2019>
- Makkink, G. F. (1957). Testing the Penman formula by means of lysimeters. *Journal of the Institution of Water Engineers*, 11(3), 277–288.
- Mauder, M., & Foken, T. (2004). *Documentation and instruction manual of the eddy covariance software package TK2* (Tech. Rep. No. Arbeitsergebnisse 26). Universität Bayreuth, Abt. Mikrometeorologie.
- Mauder, M., Foken, T., & Cuxart, J. (2020). Surface-energy-balance closure over land: A review. *Boundary-Layer Meteorology*, 177(2), 395–426. <https://doi.org/10.1007/s10546-020-00529-6>
- McMahon, T. A., Peel, M. C., Lowe, L., Srikanthan, R., & McVicar, T. R. (2013). Estimating actual, potential, reference crop and pan evaporation using standard meteorological data: A pragmatic synthesis. *Hydrology and Earth System Sciences*, 17(4), 1331–1363. <https://doi.org/10.5194/hess-17-1331-2013>
- McNaughton, K. G., & Spriggs, T. W. (1986). A mixed-layer model for regional evaporation. *Boundary-Layer Meteorology*, 34(3), 243–262. <https://doi.org/10.1007/BF00122381>
- Meijninger, W. M. L., Hartogensis, O. K., Kohsiek, W., Hoedjes, J. C. B., Zuurbier, R. M., & De Bruin, H. A. R. (2002). Determination of area-averaged sensible heat fluxes with a large aperture scintillometer over a heterogeneous surface – Flevoland field experiment. *Boundary-Layer Meteorology*, 105(1), 37–62. <https://doi.org/10.1023/A:1019647732027>
- Miralles, D. G., Brutsaert, W., Dolman, A. J., & Gash, J. H. (2020). On the use of the term “evapotranspiration”. *Water Resources Research*, 56(11), 1–5. <https://doi.org/10.1029/2020WR028055>
- Miralles, D. G., Gentile, P., Seneviratne, S. I., & Teuling, A. J. (2019). Land-atmospheric feedbacks during droughts and heatwaves: State of the science and current challenges. *Annals of the New York Academy of Sciences*, 1436(1), 19–35. <https://doi.org/10.1111/nyas.13912>
- Miralles, D. G., Teuling, A. J., van Heerwaarden, C. C., & Vilà-Guerau de Arellano, J. (2014). Mega-heatwave temperatures due to combined soil desiccation and atmospheric heat accumulation. *Nature Geoscience*, 7(5), 345–349. <https://doi.org/10.1038/ngeo2141>
- Moene, A. F., & van Dam, J. C. (2014). *Transport in the atmosphere-vegetation-soil continuum*. Cambridge University Press.
- Mol, W. B., van Stratum, B. J. H., Knap, W. H., & van Heerwaarden, C. C. (2023). Reconciling observations of solar irradiance variability with cloud size distributions. *Journal of Geophysical Research: Atmospheres*, 128(5), e2022JD037894. <https://doi.org/10.1029/2022JD037894>
- Monteith, J. L. (1965). Evaporation and environment. In *Symposia of the society for experimental biology* (Vol. 19, pp. 205–234).
- Moors, E. (2012). *Water use of forests in The Netherlands* (Doctoral dissertation). Vrije Universiteit Amsterdam.
- Moors, E., Dolman, H. A., Elbers, J., Hensen, A., Duyzer, J., Kroon, P., et al. (2012). *Integrated observations and modelling of greenhouse gas budgets at the ecosystem level in The Netherlands* (Tech. Rep.). KVR 055/12: National Research Programme Climate Changes Spatial Planning.
- Muñoz Sabater, J. (2021). *ERA5-Land hourly data from 1950 to 1980*. (Tech. Rep.). Copernicus Climate Change Service (C3S). <https://doi.org/10.24381/cds.e2161bac>
- Papale, D., & Valentini, R. (2003). A new assessment of European forests carbon exchanges by eddy fluxes and artificial neural network spatialization. *Global Change Biology*, 9(4), 525–535. <https://doi.org/10.1046/j.1365-2486.2003.00609.x>
- Penman, H. L. (1948). Natural evaporation from open water, bare soil and grass. *Proceedings of the Royal Society of London. Series A. Mathematical and Physical Sciences*, 193(1032), 120–145. <https://doi.org/10.1098/rspa.1948.0037>
- Priestley, C. H. B., & Taylor, R. J. (1972). On the assessment of surface heat flux and evaporation using large-scale parameters. *Monthly Weather Review*, 100(2), 81–92. [https://doi.org/10.1175/1520-0493\(1972\)100<0081:OTAOSH>2.3.CO;2](https://doi.org/10.1175/1520-0493(1972)100<0081:OTAOSH>2.3.CO;2)

- Savenije, H. H. G. (2004). The importance of interception and why we should delete the term evapotranspiration from our vocabulary. *Hydrological Processes*, 18(8), 1507–1511. <https://doi.org/10.1002/hyp.5563>
- Schilperoort, B., Coenders-Gerrits, M., Luxemburg, W., Jiménez Rodríguez, C., Cisneros Vaca, C., & Savenije, H. (2018). Technical note: Using distributed temperature sensing for Bowen ratio evaporation measurements. *Hydrology and Earth System Sciences*, 22(1), 819–830. <https://doi.org/10.5194/hess-22-819-2018>
- Seneviratne, S. I., Corti, T., Davin, E. L., Hirschi, M., Jaeger, E. B., Lehner, I., et al. (2010). Investigating soil moisture–climate interactions in a changing climate: A review. *Earth-Science Reviews*, 99(3), 125–161. <https://doi.org/10.1016/j.earscirev.2010.02.004>
- Steenneveld, G.-J., Horst, S., & Heusinkveld, B. (2020). Observing the surface radiation and energy balance, carbon dioxide and methane fluxes over the city centre of Amsterdam. In *EGU general assembly*. <https://doi.org/10.5194/egusphere-egu2020-1547>
- Steenneveld, G. J., Tolk, L. F., Moene, A. F., Hartogensis, O. K., Peters, W., & Holtslag, A. A. M. (2011). Confronting the WRF and RAMS mesoscale models with innovative observations in The Netherlands: Evaluating the boundary layer heat budget. *Journal of Geophysical Research*, 116(D23), 1–16. <https://doi.org/10.1029/2011JD016303>
- Teuling, A. J. (2018). A forest evapotranspiration paradox investigated using lysimeter data. *Vadose Zone Journal*, 17(1), 1–7. <https://doi.org/10.2136/vzj2017.01.0031>
- Teuling, A. J., Hirschi, M., Ohmura, A., Wild, M., Reichstein, M., Ciais, P., et al. (2009). A regional perspective on trends in continental evaporation. *Geophysical Research Letters*, 36(2), 1–5. <https://doi.org/10.1029/2008GL036584>
- Teuling, A. J., Seneviratne, S. I., Stöckli, R., Reichstein, M., Moors, E., Ciais, P., et al. (2010). Contrasting response of European forest and grassland energy exchange to heatwaves. *Nature Geoscience*, 3(10), 722–727. <https://doi.org/10.1038/ngeo950>
- Teuling, A. J., Seneviratne, S. I., Williams, C., & Troch, P. A. (2006). Observed timescales of evapotranspiration response to soil moisture. *Geophysical Research Letters*, 33(23), 1–5. <https://doi.org/10.1029/2006GL028178>
- Thornthwaite, C. W. (1948). An Approach toward a rational classification of climate. *Geographical Review*, 38(1), 55–94. <https://doi.org/10.2307/210739>
- TNO. (2022). DINoloket - Data and information on the Dutch subsurface.
- Van der Laan, S. (2010). *Validation of the greenhouse gas balance of The Netherlands. Observational constraints on CO<sub>2</sub>, CH<sub>4</sub> and N<sub>2</sub>O from atmospheric monitoring station Lutfjewad. (Unpublished doctoral dissertation)*. University of Groningen. Retrieved from <http://www.rug.nl/>
- Van der Velde, Y., Lyon, S. W., & Destouni, G. (2013). Data-driven regionalization of river discharges and emergent land cover–evapotranspiration relationships across Sweden. *Journal of Geophysical Research: Atmospheres*, 118(6), 2576–2587. <https://doi.org/10.1002/jgrd.50224>
- Van Dijk, A. I. J. M., Gash, J. H., van Gorsel, E., Blanken, P. D., Cescatti, A., Emmel, C., et al. (2015). Rainfall interception and the coupled surface water and energy balance. *Agricultural and Forest Meteorology*, 214–215, 402–415. <https://doi.org/10.1016/j.agrformet.2015.09.006>
- Van Heerwaarden, C., & Teuling, A. (2014). Disentangling the response of forest and grassland energy exchange to heatwaves under idealized land-atmosphere coupling. *Biogeosciences*, 11(21), 6159–6171. <https://doi.org/10.5194/bg-11-6159-2014>
- Vercauteren, N., Bou-Zeid, E., Huwald, H., Parlange, M. B., & Brutsaert, W. (2009). Estimation of wet surface evaporation from sensible heat flux measurements. *Water Resources Research*, 45(6), 1–7. <https://doi.org/10.1029/2008WR007544>
- Vilà-Guerau de Arellano, J., Ney, P., Hartogensis, O., de Boer, H., van Diepen, K., Emin, D., et al. (2020). CloudRoots: Integration of advanced instrumental techniques and process modelling of sub-hourly and sub-kilometre land–atmosphere interactions. *Biogeosciences*, 17(17), 4375–4404. <https://doi.org/10.5194/bg-17-4375-2020>
- Voortman, B. R., Bartholomeus, R. P., van der Zee, S. E. A. T. M., Bierkens, M. F. P., & Witte, J. P. M. (2015). Quantifying energy and water fluxes in dry dune ecosystems of The Netherlands. *Hydrology and Earth System Sciences*, 19(9), 3787–3805. <https://doi.org/10.5194/hess-19-3787-2015>
- Wang-Erlandsson, L., van der Ent, R. J., Gordon, L. J., & Savenije, H. H. G. (2014). Contrasting roles of interception and transpiration in the hydrological cycle – Part I: Temporal characteristics over land. *Earth System Dynamics*, 5(2), 441–469. <https://doi.org/10.5194/esd-5-441-2014>
- Williams, C. A., & Albertson, J. D. (2004). Soil moisture controls on canopy-scale water and carbon fluxes in an African savanna. *Water Resources Research*, 40(9), 1–14. <https://doi.org/10.1029/2004WR003208>
- Williams, C. A., Reichstein, M., Buchmann, N., Baldocchi, D., Beer, C., Schwalm, C., et al. (2012). Climate and vegetation controls on the surface water balance: Synthesis of evapotranspiration measured across a global network of flux towers. *Water Resources Research*, 48(6), 1–13. <https://doi.org/10.1029/2011WR011586>
- Wilson, K. B., Baldocchi, D. D., Aubinet, M., Berbigier, P., Bernhofer, C., Dolman, H., et al. (2002). Energy partitioning between latent and sensible heat flux during the warm season at FLUXNET sites. *Water Resources Research*, 38(12), 1–11. <https://doi.org/10.1029/2001WR000989>
- Xiao, J., Zhuang, Q., Law, B. E., Baldocchi, D. D., Chen, J., Richardson, A. D., et al. (2011). Assessing net ecosystem carbon exchange of U.S. terrestrial ecosystems by integrating eddy covariance flux measurements and satellite observations. *Agricultural and Forest Meteorology*, 151(1), 60–69. <https://doi.org/10.1016/j.agrformet.2010.09.002>
- Xu, R., Li, Y., Teuling, A. J., Zhao, L., Spracklen, D. V., Garcia-Carreras, L., et al. (2022). Contrasting impacts of forests on cloud cover based on satellite observations. *Nature Communications*, 13(1), 670. <https://doi.org/10.1038/s41467-022-28161-7>
- Zhang, K., Kimball, J. S., Nemani, R. R., Running, S. W., Hong, Y., Gourley, J. J., & Yu, Z. (2015). Vegetation greening and climate change promote multidecadal rises of global land evapotranspiration. *Scientific Reports*, 5(1), 15956. <https://doi.org/10.1038/srep15956>